Articles

Insight into the Structural Requirements of Urokinase-Type Plasminogen Activator Inhibitors Based on 3D QSAR CoMFA/CoMSIA Models

Bhoomendra A. Bhongade[†] and Andanappa K. Gadad*[,†,‡]

Department of Medicinal Chemistry, College of Pharmacy, J. N. Medical College, Belgaum-590 010, Karnataka, India, and Pharmacy Program, Faculty of Medical Sciences, The University of The West Indies, St. Augustine, Champs Fleurs, Mount Hope, Trinidad, WI

Received February 15, 2005

Urokinase-type plasminogen activator (uPA), a trypsin-like serine protease, has been implicated in large number of malignancies, tumor cell invasion, angiogenesis and metastasis; hence, the potent and selective inhibitors of uPA may therefore be therapeutically useful drugs for treatment of various forms of cancer. A three-dimensional quantitative structure−activity relationship (3D QSAR) study was performed on five different chemical series reported as selective uPA inhibitors employing comparative molecular field analysis (CoMFA)/comparative molecular similarity indices analysis (CoMSIA) techniques to investigate the structural requirements for substrates and derive a predictive model that may be used for the design of novel uPA inhibitors. ClogP has been used as an additional descriptor in the CoMFA analysis to study the effects of lipophilic parameters on activity. Inclusion of ClogP did not improve the models significantly and exhibited comparable correlation coefficients with CoMFA steric and electrostatic models. 3D QSAR models were derived for 2-pyridinylguanidines (training set $N = 25$, test set $N = 8$), 4-aminoarylguanidines and 4-aminoarylbenzamidines (training set $N = 29$, test set $N = 8$), thiophene-2-carboxamindines (training set $N = 64$, test set $N = 19$), 2-naphthamidines (training set $N = 32$, test set $N = 8$), and 1-isoquinolinylguanidines (training set $N = 29$, test set $N = 7$). The CoMFA models with steric and electrostatic fields exhibited r^2_{cv} 0.452−0.722, r^2_{ncv} 0.812−0.986, r^2_{pred} 0.597−0.870, whereas CoMFA ClogP models showed r^2_{cv} 0.420−0.707, r^2_{ncv} 0.849−0.957, r^2_{pred} 0.600−0.870. The CoMSIA models displayed r^2_{cv} 0.663−0.729, r^2_{ncv} 0.909−0.998, r^2_{pred} 0.554−0.855. 3D contour maps generated from these models were analyzed individually, which provides the regions in space where interactive fields may influence the activity. The superimposition of contour maps on the active site of serine proteases additionally helps in understanding the structural requirements of these inhibitors. Further, the predictive ability of 3D QSAR models was affirmed by predicting the activity of novel 2-naphthamidines. 3D QSAR models developed may be used in designing and predicting the uPA inhibitory activity of novel molecules.

Introduction

It is widely documented that the progression of cancer cell invasion and metastasis is hinged on the ability of tumor cells to produce and recruit proteolytic enzymes. Among the diverse proteolytic enzyme systems produced by human cancers, the plasminogen activator−plasmin system is preferentially involved in cancer cell invasion and metastasis.[1] The plasminogen activators are a group of serine proteolytic enzymes existing mainly as urokinase-type plasminogen activator (uPA) and tissue-type plasminogen activator (tPA).[2]

uPA, a trypsin-like serine protease, is the key initiator of the extracellular proteolytic cascade driving cellular invasiveness.[3] Proteolytically active uPA is a disulfide-linked two-chain protein generated from proteolytically inactive pro-uPA by the hydrolysis of the Lys158-Ile159 peptide bond.[4] The central role of uPA is to convert plasminogen to plasmin, which digests the components of the extracellular matrix and basement membranes either directly or by activation of proenzymes of matrix metalloproteinases.[3,5] Urokinase secreted by tumor cells or the adjacent stroma exists as free enzyme or bound to the cell surface receptor, uPAR. Binding to uPAR significantly increases the rate of cell surface-associated plasminogen activation by urokinase and can serve to spatially focus its activity. The uPA/uPAR complex displays a vital role not only in normal physiological events of wound healing but is also involved in tissue remodeling of various diseases including arthritis, atherosclerosis, vascular restenosis and cancer.[6−8] uPA in particular is implicated in various malignancies including cancer of breast, lung, bladder, stomach, cervix, kidney, etc. Higher levels of urokinase have been correlated with poor patient prognosis and also implicated in extracellular matrix degradation, tumor cell invasion, angiogenesis and metastasis.[9,10] The role of the plasminogen activator system in various cancers was reviewed extensively.[11] The closely related enzyme, tPA, also functions via activation of plasminogen to plasmin and is the key component of the fibrinolytic cascade.[12] Hence, it is essential that uPA inhibitors should exhibit adequate potency and selectivity toward uPA relative to tPA and plasmin in order to avoid the possibility of antifibrinolytic side effects.

The small molecule inhibitors of uPA contain an amidino or guanidino, positively charged arginine-mimetic groups that form a salt bridge with Asp189 carboxylate in the S1 pocket of the urokinase active site and other trypsin-like serine proteases. The

* Corresponding author. Tel.: 1 868 662147, 91 831 2471399; Fax: 91 831 2472387, E-mail: akgadad@rediffmail.com, babhongade@rediffmail.com.
[†] J. N. Medical College, College of Pharmacy.
[‡] The University of The West Indies.

10.1021/jm050149r CCC: $33.50
Published on Web 12/23/2005

previously reported uPA inhibitors were arylamidines,[13] guanidines[14] with minimal substitutions, and amiloride.[15] Novel selective uPA inhibitors include benzo(*b*)thiophene-2-carboxamidines,[16] indole/benzoimidazole-5-carboxamidines,[17] 2-pyridinylguanidines,[18] 4-aminoarylguanidines/benzamidines,[19] thiophene-2-carboxamidines,[20] 2-naphthamidines,[21] 1-isoquinolinylguanidines,[22] 2-aminobenzimidazoles,[23] etc. Some of these inhibitors exhibit binding constants in the nanomolar range and are still being developed as drug candidates. No significant breakthrough has occurred in achieving the essential requirements for a therapeutic agent in the treatment of cancer based on uPA inhibition.

Structure-based drug design (SBDD) using crystals of uPA in complex with ligands is expected to greatly accelerate the inhibitor optimization process.[24] It has been found that these inhibitors bind to a specific pocket of uPA in a different way, targeting new subsites (S1β, S1′, etc). The challenging task in SBDD of uPA inhibitors is not only to optimize the binding of inhibitors to their respective subsites, but also to combine the successful functionalities of different inhibitors in a single molecule. Hence, the comprehensive quantitative structure−activity relationship data may be critical in designing novel molecules.

Previously, we have reported the 3D QSAR models for a series of indole/benzoimidazole-5-carboxamidines as uPA and other trypsin-like serine protease inhibitors.[25] The present study is aimed at elucidating the structural features required for uPA inhibition and to obtain predictive three-dimensional quantitative structure−activity relationship (3D QSAR) models, which may guide the rational synthesis of novel compounds. In the present paper, we report the 3D QSAR models derived using the most widely used computational tools, comparative molecular field analysis (CoMFA)/comparative molecular similarity indices analysis (CoMSIA) methods,[26,27] for five different chemical series of uPA inhibitors from the literature. CoMFA and CoMSIA methods have been the most powerful tools in the 3D QSAR approach and are used in understanding the mechanism of interaction between various receptors and ligands. ClogP[28] has been used as an additional descriptor in CoMFA analysis, which accounts for hydrophobic interactions between ligand and receptor as well as in the random walk process in the organism from the site of injection to the site of action.

The derived 3D QSAR CoMFA and CoMSIA models for different chemical series reported as uPA inhibitors[18−22] give insight to the influence of various interactive fields on the activity and thus aid in designing and forecasting the uPA inhibitory activity of novel molecules.

Materials and Methods

Data Set. The training and test set used in the computational studies comprises of molecules belonging to various chemical classes reported as uPA inhibitors. The uPA inhibitory data has been collected from the literature.[18−22] The in vitro inhibitory activity K_i (μM) against uPA converted to pK_i (μM, pK_i = log 1/K_i) was used as dependent variable in deriving 3D QSAR models. The structures and biological activity data of training and test set molecules are described in Tables S1−S5 (see Supporting Information).

Molecular Modeling. All computational studies were performed using Sybyl 6.7[29] (Tripos Inc.) software running on Silicon Graphics Indy o2 workstation. The 3D structures of molecules were constructed by modification of X-ray crystal structures obtained from the protein data bank (4-aminoarylguanidines: 1ejn; 2-naphthamidines: 1owd, 1owj, 1sqa, 1sqo, 1owe, 1owh, 1owj, 1owk; thiophene-2-carboxamidines: 1o5b) and 4-aminoarylguanidines, 2-pyridinylguanidines and 1-isoquinolinylguanidines were built using the Sketch Molecule function with Sybyl. Initial optimization of the structures was carried out using TRIPOS force field with the Gasteiger Huckel charges, and repeated minimization was performed using steepest descent and conjugated gradient method till the root-mean-square (rms) deviation of 0.001 kcal/mol was achieved. The minimized structures were subjected to a systematic search routine of all rotatable bonds in 10° increments from 0° to 359°. Conformational energies were computed with electrostatic terms; the lowest energy structures finally minimized were used in superimpositions. The partial atomic charges required for the electrostatic interaction were computed by a semiempirical molecular orbital method using MOPAC[30] with AM1 Hamiltonian[31] (Key word: DEBUG).

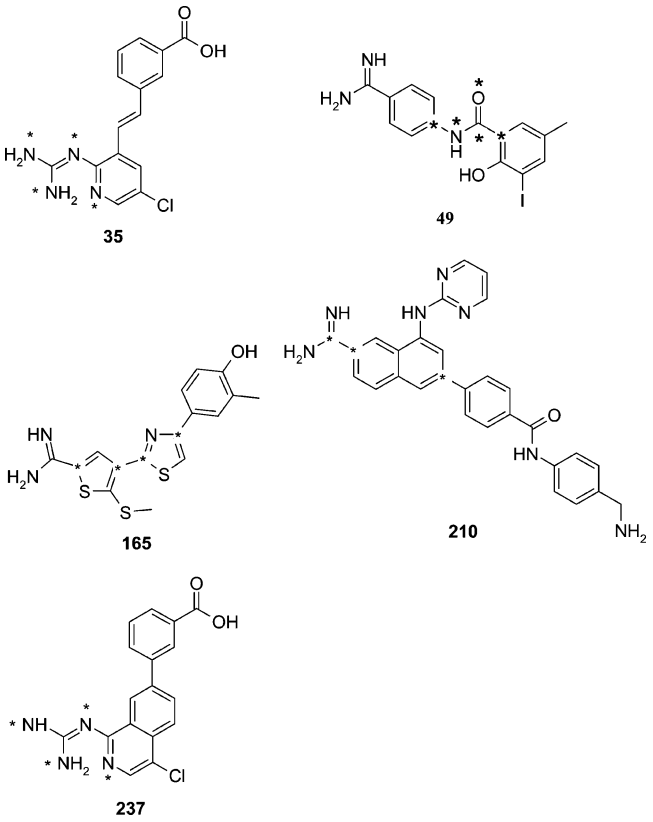

Figure 1. Template structures and (hetero)atoms used in the rms alignment.

Development of predictive 3D QSAR CoMFA models is essentially alignment sensitive that defines the putative pharmacophore for the series of ligands under investigation. Two different approaches of alignment were used to calculate the CoMFA/CoMSIA probe interaction energies. In the first alignment the (hetero)atoms of molecules were used for rms fitting (Figure 1), and in the second alignment, each analogue was aligned to the template by rotation and translation so as to minimize rmsd between the atoms in the template and the corresponding atoms in the analogue using the database align command within Sybyl. The view of the data set molecules from rms alignment superimposed on crystal structures are displayed in Figures S1−S5.

CoMFA and CoMSIA Analyses. CoMFA steric and electrostatic field energies were calculated using the sp^3 carbon probe atom with a van der Waals radius of 1.52 Å and +1 charge. The energies were truncated to ± 30 kcal/mol, and the electrostatic contributions were ignored at the lattice intersection with maximal steric interactions. The CoMFA fields generated were automatically scaled by the CoMFA-STD method in Sybyl.

The CoMSIA method involves a common probe atom and similarity indices calculated at regularly spaced grid intervals for the prealigned molecules. The similarity indices descriptors were derived with the same lattice box used in CoMFA. CoMSIA calculates hydrophobic, H-bond donor and acceptor fields in

Table 1. Summary of CoMFA Results from Atom-Based rms Alignment

	I[a]		II[b]		III[c]		IV[d]		V[e]	
	SE	ClogP	SE	ClogP	SE	ClogP	SE	ClogP	SE	ClogP
r^2_{cv}	0.722	0.673	0.672	0.634	0.452	0.420	0.672	0.619	0.641	0.707
N_c	1	2	6	6	5	6	6	5	1	2
SEP	0.342	0.536	0.607	0.641	0.396	0.411	1.019	1.077	0.368	0.343
r^2_{ncv}	0.825	0.860	0.968	0.959	0.925	0.929	0.986	0.956	0.812	0.849
SEE	0.257	0.351	0.194	0.212	0.147	0.144	0.211	0.366	0.267	0.246
F value	80.272	67.594	90.479	86.249	142.651	124.712	292.186	112.927	73.441	44.906
P $r^2_{=0}$	0	0	0	0	0	0	0	0	0	0
					Contribution (%)					
S	72.2	48.1	57.9	58.1	57.5	56.5	53.1	52.7	56.8	66.1
E	27.8	31.9	42.1	40.9	42.5	42.7	46.9	45.2	43.2	28.5
ClogP	-	20.0	-	1.0	-	0.8	-	2.1	-	5.4
r^2_{pred}	0.870	0.600	0.642	0.743	0.597	0.608	0.867	0.878	0.673	0.619
r^2_{bs}	0.835	0.902	0.988	0.980	0.952	0.953	0.993	0.981	0.830	0.885
std dev	0.053	0.037	0.009	0.010	0.012	0.013	0.003	0.006	0.055	0.031

[a] 2-Pyridinylguanidines. [b] 4-Aminoarylguanidines and 4-aminobenzamidines. [c] Thiophene-2-carboxamidines. [d] 2-Naphthamidines. [e] 1-Isoquinolinylguanidines.

Table 2. Summary of CoMSIA Results for 2-Pyridinylguanidines[a]

	SE	SED	SEA	SEH	SEDA	SEHD	SEHA	SEHDA
r^2_{cv}	0.658	0.627	0.615	0.727	0.643	0.741	0.661	0.696
N_c	5	13	8	7	13	10	9	9
SEP	0.590	0.809	0.682	0.556	0.785	0.598	0.661	0.625
r^2_{ncv}	0.979	0.999	0.992	0.996	0.998	0.999	0.998	0.998
SEE	0.147	0.037	0.096	0.066	0.055	0.040	0.049	0.052
F value	147.851	1060.74	257.541	627.257	484.442	1183.32	896.165	789.200
P $r^2_{=0}$	0	0	0	0	0	0	0	0
				Contribution (%)				
S	41.2	34.2	25.1	24.9	20.2	23.0	19.9	18.0
E	58.8	46.1	37.6	43.6	34.8	34.7	26.3	23.8
ClogP	-	-	-	-	-	-	-	-
H	-	-	-	31.4	-	28.0	23.3	21.4
D	-	19.7	-	-	14.0	14.3	-	10.3
A	-	-	37.4	-	31.0	-	30.5	26.5
r^2_{pred}	0.253	0.582	0.653	0.431	0.735	0.651	0.786	0.851
r^2_{bs}	0.989	1.000	0.995	0.998	1.000	1.000	0.999	0.999
std dev	0.005	0	0.003	0.002	0	0	0.001	0.001

[a] S = steric, E = electrostatic, H = hydrophobic, D = H-bond donor, A = H-bond acceptor.

addition to steric and electrostatic fields. The distance dependence between the grid point and each atom of molecule was determined by Guassian function through the similarity indices calculated at all grid points, and a default value of 0.3 was used as an attenuation factor.

Partial Least Square (PLS) Analysis. The CoMFA/CoMSIA descriptors served as independent variables and pK_i (μM) values as dependent variables in PLS regression analysis for deducing 3D QSAR models.[32] Normally cross-validation is used to check the predictivity of the derived model. The result of analysis corresponds to the regression equation with thousands of coefficients. The predictive values of models were evaluated using leave-one-out (LOO) cross validation method. The number of components leading to the highest cross-validated r^2 and lowest standard error of prediction (SEP) was set as the optimum number of components (N_c) in PLS analyses. σ minimum of 2.0 kcal/mol was used as the threshold column filtering value in PLS analysis. To obtain the statistical confidence limit in the analyses, PLS analysis using 100 bootstrap groups with an optimum number of components was performed.

Predictive Ability of CoMFA and CoMSIA Models. The predictive ability of each analysis was determined from test set molecules that were not included in the training set. These molecules were aligned, and their activities were predicted by each PLS analysis. The predictive r^2 (r^2_{pred}) value defined as:

$$r^2_{pred} = (SD - PRESS)/SD$$

where SD is the sum of squared deviations between the biological activities of the test set and mean activity of the training set molecules, and PRESS is the sum of squared deviation between actual and predicted activities of the test set molecules.

Calculation of ClogP. ClogP calculated using ChemDraw Ultra 6.0 software[33] integrated with CambridgeSoft Software Development Kit (CambridgeSoft Corporation) was included with CoMFA fields.

Results and Discussion

The 3D QSAR models derived using CoMFA and CoMSIA methodologies were characterized by different chemical classes published in the literature.[18−22] The structures and biological activity data of the molecules are described in Tables S1−S5 (see Supporting Information). The in vitro uPA inhibitory activity values pK_i (μM) was used as the dependent variable and CoMFA/CoMSIA fields as independent variables in the study. The low energy conformer obtained from systematic search routine was used in the molecular alignment performed from two approaches: atom-based rms fitting on the template structures and rmsd-based database fitting. One of the major obstacles in the 3D QSAR studies lies with the 'congeners', which misfit the final equation and were termed as outliers. The reasons for the poor prediction may be their structural uniqueness, the insignificant mathematical value in defining the biological activity or varied rates of metabolism. Exceptions are also observed wherein experimentally observed parameters might be better than the calculated or vice versa; however, their inclusion in 3D QSAR studies at the cost of lower r^2 could be more confusing than helpful. The poorly predicted molecules from non-cross-validated PLS analysis as well as the compounds whose activity has not been described in specific numeric terms in the literature are also identified as outliers in

Table 3. Summary of CoMSIA Results for 4-Aminoarylguanidines and 4-Aminobenzamidines[a]

	SE	SED	SEA	SEH	SEDA	SEHD	SEHA	SEHDA
r^2_{cv}	0.587	0.679	0.682	0.635	0.679	0.649	0.650	0.663
N_c	5	4	5	10	5	5	6	6
SEP	0.666	0.574	0.584	0.707	0.586	0.614	0.626	0.615
r^2_{cv}	0.883	0.907	0.902	0.972	0.927	0.910	0.942	0.943
SEE	0.354	0.309	0.325	0.197	0.279	0.311	0.255	0.253
F value	34.725	58.764	42.228	61.907	58.711	46.407	59.580	60.493
P $r^2_{=0}$	0	0	0	0	0	0	0	0
				Contribution (%)				
S	37.5	27.9	34.2	25.4	27.6	24.0	24.9	20.5
E	62.5	38.5	33.9	37.8	24.8	23.9	24.8	19.1
ClogP	-	-	-	-	-	-	-	-
H	-	-	-	36.8	-	24.6	25.0	19.0
D	-	33.6	-	-	28.7	27.5	-	25.2
A	-	-	31.9	-	18.9	-	25.3	16.1
r^2_{pred}	0.424	0.561	0.545	0.556	0.586	0.672	0.639	0.621
r^2_{bs}	0.927	0.942	0.939	0.992	0.960	0.958	0.967	0.971
std dev	0.048	0.026	0.030	0.007	0.021	0.020	0.018	0.017

[a] S = steric, E = electrostatic, H = hydrophobic, D = H-bond donor, A = H-bond acceptor.

Table 4. Summary of CoMSIA Results for 2-Naphthamidines[a]

	SE	SED	SEA	SEH	SEDA	SEHD	SEHA	SEHDA
r^2_{cv}	0.745	0.751	0.763	0.695	0.750	0.736	0.715	0.729
N_c	4	5	7	6	5	5	5	5
SEP	0.882	0.887	0.901	1.002	0.891	0.914	0.951	0.926
r^2_{ncv}	0.895	0.951	0.967	0.961	0.955	0.961	0.956	0.959
SEE	0.565	0.394	0.285	0.357	0.377	0.353	0.373	0.359
F value	57.737	100.764	141.819	103.389	110.662	127.297	113.153	122.254
P $r^2_{=0}$	0	0	0	0	0	0	0	0
				Contribution (%)				
S	68.8	39.3	39.3	42.3	27.4	32.6	19.0	22.4
E	31.2	18.9	21.7	24.3	15.3	16.1	17.0	13.0
ClogP	-	-	-	-	-	-	-	-
H	-	-	-	33.3	-	21.7	20.3	15.9
D	-	37.5	-	-	27.6	29.7	-	23.2
A	-	-	39.0	-	29.8	-	33.7	25.4
r^2_{pred}	0.889	0.932	0.847	0.807	0.857	0.962	0.799	0.855
r^2_{bs}	0.941	0.975	0.991	0.982	0.979	0.979	0.980	0.980
std dev	0.022	0.009	0.005	0.007	0.009	0.008	0.009	0.008

[a] S = steric, E = electrostatic, H = hydrophobic, D = H-bond donor, A = H-bond acceptor.

Table 5. Summary of CoMSIA Results for 1-Isoquinolinylguanidines[a]

	SE	SED	SEA	SEH	SEDA	SEHD	SEHA	SEHDA
r^2_{cv}	0.752	0.756	0.720	0.743	0.710	0.759	0.681	0.672
N_c	5	4	12	8	10	9	1	2
SEP	0.350	0.335	0.548	0.406	0.483	0.415	0.347	0.363
r^2_{ncv}	0.976	0.969	0.995	0.995	0.992	0.998	0.860	0.909
SEE	0.109	0.120	0.071	0.056	0.082	0.042	0.230	0.191
F value	106.219	107.864	104.623	257.652	93.705	400.337	104.239	80.369
P $r^2_{=0}$	0	0	0	0	0	0	0	0
				Contribution (%)				
S	18.2	18.2	15.0	16.7	11.7	16.0	26.1	25.0
E	81.8	66.5	61.3	62.5	53.4	50.7	30.7	34.2
ClogP	-	-	-	-	-	-	-	-
H	-	-	-	20.8	-	20.2	12.7	12.4
D	-	15.3	-	-	8.7	13.1	-	4.6
A	-	-	23.7	-	26.2	-	30.5	23.7
r^2_{pred}	0.803	0.752	0.746	0.855	0.755	0.825	0.491	0.554
r^2_{bs}	0.989	0.980	1.000	0.999	0.999	1.000	0.853	0.928
std dev	0.007	0.010	0	0.001	0.002	0	0.057	0.026

[a] S = steric, E = electrostatic, H = hydrophobic, D = H-bond donor, A = H-bond acceptor.

the present study. The structural uniqueness and composition of training set molecules might be the reason for their poor prediction.

3D QSAR models were generated from training set molecules and validated by predicting activity of test set molecules. All the cross-validated results were analyzed by considering the fact that the value of r^2_{cv} above 0.3 indicates that the probability of chance correlation is less than 5%. The results of PLS analyses are summarized from CoMFA studies in Table 1 and that from the CoMSIA studies in Tables 2−5.

CoMFA Models. CoMFA models derived from atom-based rms alignment yielded better models as compared to the rmsd-based database alignment method. Other physicochemical properties of the molecules viz. hydrophobicity which may account for transport phenomenon and pharmacokinetic profile has been included in the CoMFA studies. As the biological data used in the study was in vitro enzyme inhibition, which could have contributions of hydrophobic parameters along with with the steric and electrostatic fields. Hence, to study the effects of hydrophobic/lipophilic properties of molecules on uPA inhibi-

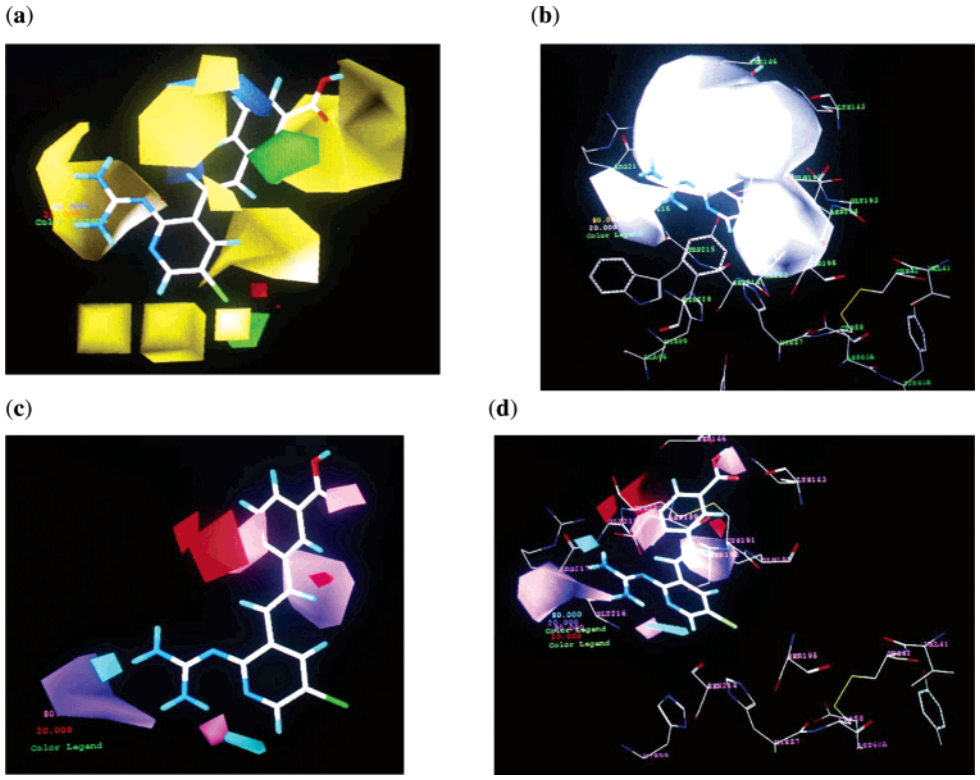

Figure 2. STDDEV*COEFF contour plots for 2-pyridinylguanidines. (a) CoMFA steric (green polyhedron: sterically favored; yellow polyhedron: sterically disfavored) and electrostatic (red polyhedron: negatively charge favored; blue polyhedron: positively charge favored). (b) CoMSIA hydrophobic (yellow: favored, white: disfavored) superimposed on uPA active sites. (c) CoMSIA H-bond donor (cyan: favored, purple: disfavored) and H-bond acceptor (magenta: favored, red: disfavored). (d) CoMSIA H-bond donor and acceptor superimposed on uPA active sites. The compound **35** in cap and stick is shown.

tory activity, we have included ClogP as an additional descriptor in the CoMFA analysis. The CoMFA ClogP models developed were statistically significant and exhibited low to moderate lipophilic contributions as compared to CoMFA models with steric and electrostatic fields. Thus, the CoMFA models generated using atom-based rms alignment with steric and electrostatic fields were considered in the generation of contour maps and in explaining SAR.

2-Pyridinylguanidines. 3D QSAR models for 2-pyridinylguanidines reported by Barber et al.[18] as selective uPA inhibitors (Table S1) were developed using 25 training set molecules and validated by predicting activity for eight test set molecules. The CoMFA model developed from steric and electrostatic fields yielded cross-validated r^2 (r^2_{cv}) 0.722 at first component, non-cross-validated r^2 (r^2_{ncv}) 0.825, predictive r^2 (r^2_{pred}) 0.780 and higher contribution of steric field (72.2%) than electrostatic (27.8%) field. Figure 2a depicts CoMFA steric and electrostatic contour plots, and Figure 3a shows the graph of actual versus fitted/predicted activities for training/test set molecules. CoMFA ClogP model showed r^2_{cv} 0.673, with r^2_{ncv} 0.860 and predictive r^2 0.600 and significant contribution of lipophilic parameters (20.0%).

4-Aminoarylguanidines and 4-Aminobenzamidines. 4-Aminoarylguanidines and 4-aminobenzamidines developed by Spancer et al.[19] as uPA inhibitors have been used to generate 3D QSAR models from 29 training set molecules (Table S2) and validated by predicting activities of eight test molecules. The CoMFA model from the contribution of steric and electrostatic fields showed r^2_{cv} 0.672 with six components, r^2_{ncv} 0.968, r^2_{pred} 0.642, the respective steric and electrostatic field contributions were 57.9% and 42.1%. The 3D contour maps generated from the above CoMFA model are shown in Figure 4a, and a graph

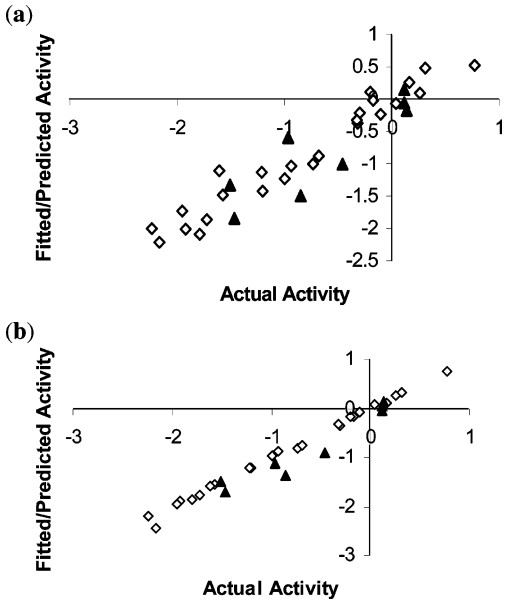

Figure 3. A graph of actual versus fitted/predicted activities for training and test set molecules of 2-pyridinylguanidines. (a) CoMFA. (b) CoMSIA (◇ training set; ▲ test set).

of actual versus fitted/predicted activities for training/test set molecules is exhibited in Figure 5a. The CoMFA ClogP model yielded r^2_{cv} 0.634 with six components, r^2_{ncv} 0.959 with improved predictive r^2 value 0.743.

Thiophene-2-carboxamidines. Thiophene-2-carboxamidines[20] (Table S3) with selective uPA inhibitory activity developed by a research group of 3D Pharmaceuticals were used in the generation of 3D QSAR models from a training set comprising

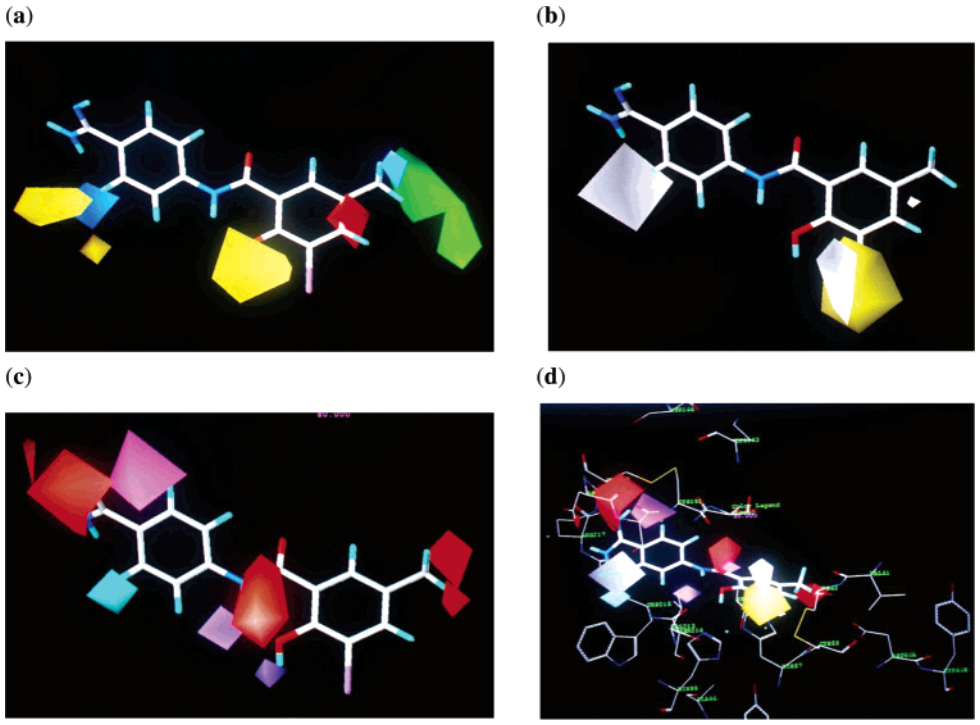

Figure 4. STDDEV*COEFF contour plots for 4-aminoarylguanidines and 4-aminobenzamidines. (a) CoMFA steric and electrostatic. (b) CoMSIA hydrophobic. (c) CoMSIA H-bond donor and acceptor. (d) CoMSIA hydrophobic, H-bond donor and acceptor fields superimposed on uPA active sites. The compound **49** in cap and stick is shown.

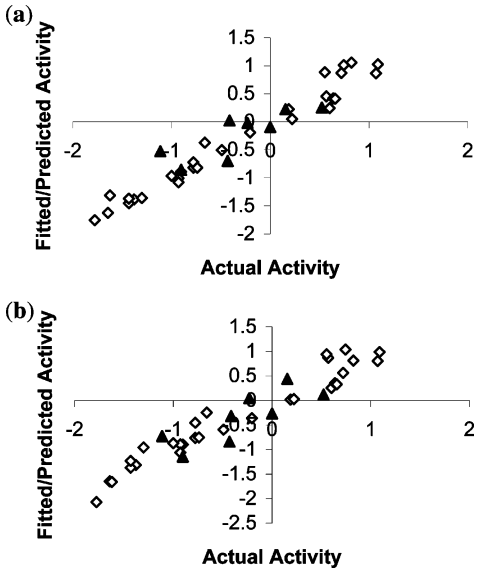

Figure 5. A graph of actual versus fitted/predicted activities for training and test set molecules of 4-aminoarylguanidines and 4-aminobenzamidines. (a) CoMFA. (b) CoMSIA (◇ training set; ▲ test set).

64 molecules and validated by 19 test set molecules. A combination of steric and electrostatic fields yielded the CoMFA model having r^2_{cv} 0.452 with five components, r^2_{ncv} 0.925, predictive r^2 0.597 and exhibited higher steric field contribution (57.5%). The 3D steric and electrostatic contour map is depicted in Figures 6a and 6b, respectively, and the graph of actual versus fitted/predicted activities for training/test set molecules is shown in Figure 7. The CoMFA model obtained using additional descriptor ClogP improved external predictions. This model exhibited r^2_{cv} 0.420 with six components, r^2_{ncv} 0.929 and predictive r^2 0.608. The steric, electrostatic and ClogP contributions were 56.5%, 42.7% and 0.8%, respectively.

2-Naphthamidines. 2-Naphthamidines reported as selective uPA inhibitors by Wendt et al.[21] have been utilized to develop 3D QSAR models from a training set comprising 32 molecules and validated with eight test set molecules (Table S4). The CoMFA steric, electrostatic and ClogP models generated were statistically significant and exhibited decreased internal and improved external predictions. The CoMFA model generated from steric and electrostatic fields was characterized by r^2_{cv} 0.672 at six components, r^2_{ncv} 0.986, predictive r^2 0.867, whereas inclusion of ClogP resulted in r^2_{cv} 0.619 with five components, r^2_{ncv} 0.956, predictive r^2 0.878 and higher contributions of steric fields toward uPA inhibitory activity. The 3D steric and electrostatic contour plots from CoMFA model are shown in Figures 8a and 8b, respectively. Graph of actual versus fitted/predicted activities for training/test set molecules is shown in Figure 9a.

1-Isoquinolinylguanidines. Selective uPA inhibitors 1-isoquinolinylguanidines (Table S5) reported by Barber et al.[22] have been used to generate 3D QSAR models employing 29 training set molecules validated by predicting activity of seven test set molecules. The CoMFA model generated from steric and electrostatic fields showed r^2_{cv} 0.641 at first component, r^2_{ncv} 0.812, predictive r^2 0.673 and higher contribution of steric field (56.8%) than the electrostatic field (43.2%). The 3D contours developed for this model and superimposed on the uPA active sites are shown in Figure 10a, and the graph of actual versus fitted/predicted activities for training/test set molecules are displayed in the Figure 11a. CoMFA ClogP model was characterized by an increased internal prediction of r^2_{cv} 0.707, r^2_{ncv} 0.849 and decreased r^2_{pred} 0.619.

CoMSIA Models. To investigate the significance of hydrophobic and H-bond fields on the uPA inhibitory activity, CoMSIA analysis using steric, electrostatic, hydrophobic and H-bond fields was carried out employing the same rms alignment used for CoMFA studies.

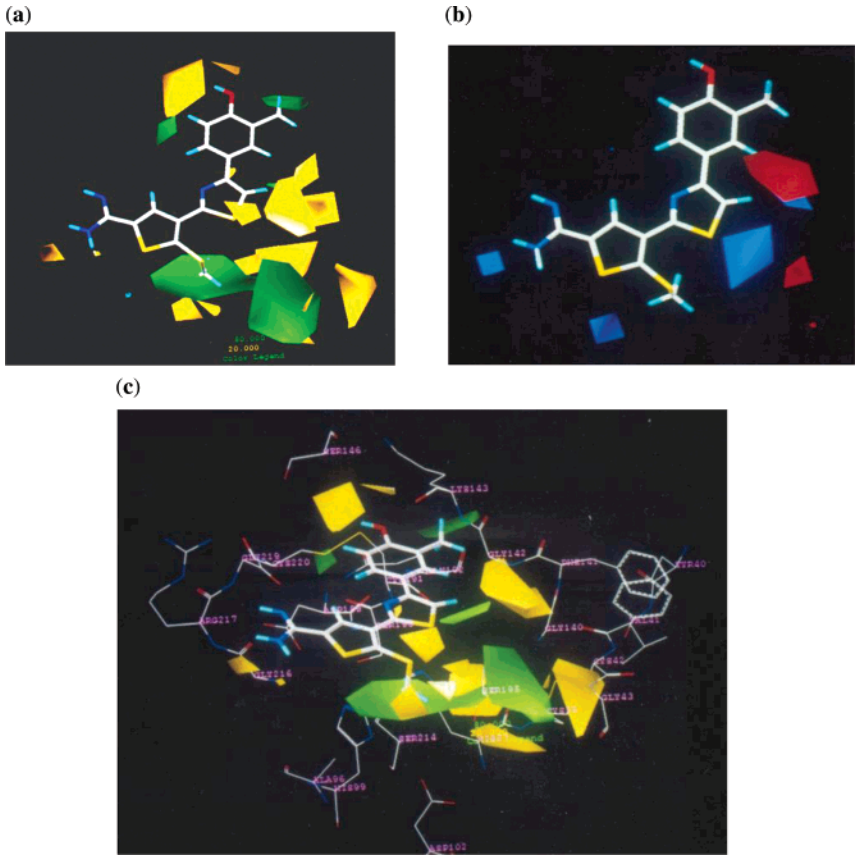

Figure 6. CoMFA steric and electrostatic STDDEV*COEFF contour plots for thiophene-2-carboxamidines. (a) CoMFA steric. (b) CoMFA electrostatic. (c) CoMFA steric and electrostatic fields superimposed on uPA active sites. Compound **165** in cap and stick is shown.

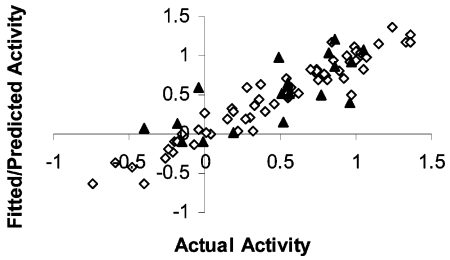

Figure 7. A graph of actual versus fitted/predicted activities for training and test set molecules of thiophene-2-carboxamidines from CoMFA model with steric and electrostatic fields. (◇ training set; ▲ test set).

2-Pyridinylguanidines. The results of CoMSIA PLS analysis are summarized in Table 2. The CoMSIA model generated from steric and electrostatic fields exhibited poor external predictions r^2_{pred} 0.253 with r^2_{cv} 0.658 at five components, r^2_{ncv} 0.979. Incorporation of the H-bond donor/acceptor or both fields yielded models with an improved external prediction, while the highest predictive r^2 value 0.735 was observed with steric, electrostatic, H-bond donor and acceptor fields. These models showed comparable predictions, but optimum number of components required to generate models were significantly higher. Hence they were considered to be of less statistical significance. The combinations of steric, electrostatic and hydrophobic fields yielded CoMSIA models with an improved r^2_{cv} 0.727 and an average predictive value of r^2 0.431. Inclusion of H-bond acceptor and donor fields showed improved predictive r^2 values of 0.786 and 0.651, respectively, indicating higher contributions of these substituents in activity, while the CoMSIA model developed with all five fields, yielded model with highest predictive r^2 0.851 and also demonstrated r^2_{cv} 0.696 with nine components, r^2_{ncv} 0.998, r^2_{bs} 0.999 with steric (18%), electrostatic (23.8%), hydrophobic (21.4%), H-bond donor (10.3%) and acceptor (26.5%) field contributions. The 3D contours analyzed using this model are shown in Figures S6b,c and Figures 2b−d. The graph of actual versus fitted/predicted activities for training/test set molecules is depicted in Figure 3b. The CoMSIA studies signify the contribution of H-bond acceptor and hydrophobic fields in addition to electrostatic and steric fields toward the uPA inhibitory activity of 2-pyridinylguanidines.

4-Aminoarylguanidines and 4-Aminobenzamidines. The results of PLS analysis for CoMSIA are summarized in Table 3. An improved internal prediction was observed for CoMSIA models obtained using steric, electrostatic, H-bond fields. The PLS analysis of CoMSIA generated from steric, electrostatic, H-bond donor and acceptor fields showed r^2_{cv} 0.679 with five components, the corresponding r^2_{ncv} as 0.927, and predictive r^2 0.586. The model generated using hydrophobic, steric and electrostic fields exhibited significant contribution of hydrophobic parameters and an improved statistical correlation coefficients r^2_{cv} 0.587−0.635, r^2_{ncv} 0.883−0.972 and predictive r^2 0.424−0.556. Further, model obtained with combination of steric, electrostatic, hydrophobic and H-bond donor fields showed r^2_{cv} 0.649, r^2_{ncv} 0.910 and highest r^2_{pred} 0.672, whereas incorporation of H-bond acceptor field to the steric, electrostatic and hydrophobic fields resulted in r^2_{cv} 0.650, r^2_{ncv} 0.942 and predictive r^2 0.639. The model generated using all five CoMSIA fields yielded statistically significant model with r^2_{cv} 0.663 for six components, r^2_{ncv} 0.943, r^2_{bs} 0.971 and r^2_{pred} 0.621 and respective field contributions was steric 20.5%, electrostatic 19.1% hydrophobic 19.0%, H-bond donor 25.2% and acceptor 16.1%. This model with good internal and external predictions was used to analyze 3D contour plots (Figures 4b−d). The plot

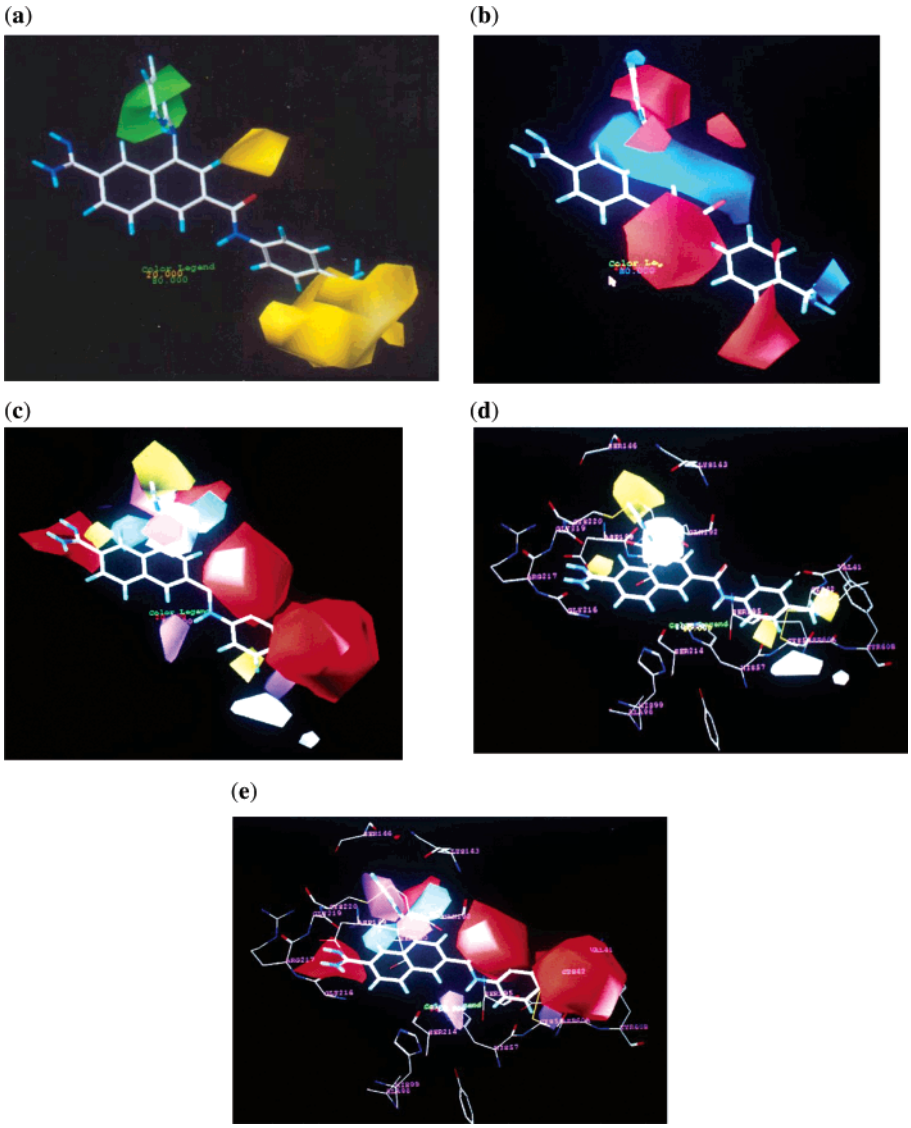

Figure 8. STDDEV*COEFF contour plots for 2-naphthamidines. (a) CoMFA steric. (b) CoMFA electrostatic. (c) CoMSIA hydrophobic, H-bond donor and acceptor. (d) CoMSIA hydrophobic superimposed on uPA active sites. (e) CoMSIA H-bond donor and acceptor superimposed on uPA active sites. Compound **210** in cap and stick is shown.

depicting actual versus fitted/predicted activities of the data set molecules is shown in Figure 5b. The analysis of CoMSIA model showed higher contributions of H-bond donor fields followed by steric, electrostatic, hydrophobic and H-bond acceptor to the uPA inhibitory activity of 4-aminoarylguanidines and 4-aminobenzamidines.

2-Naphthamidines. The models generated for 2-naphthamidines using various CoMSIA fields showed high external predictions and were statistically robust. The results obtained from CoMSIA PLS analysis are summarized in Table 4. The models developed from steric and electrostatic fields yielded r^2_{cv} 0.745 at four components with corresponding r^2_{ncv} 0.895, r^2_{pred} 0.889 and steric 68.8% and electrostatic 31.2% field contributions. The incorporation of H-bond donor and acceptor fields exhibited comparable model (r^2_{cv} 0.750, r^2_{ncv} 0.955, r^2_{pred} 0.857). Further, models developed from steric, electrostatic and hydrophobic fields resulted in decreased external predictions (r^2_{pred} 0.807) compared to steric and electrostatic model (r^2_{pred} 0.889), whereas steric, electrostatic, hydrophobic and H-bond donor fields exhibited the highest predictive r^2 0.962. The CoMSIA model generated with all the five fields exhibited r^2_{cv} 0.729 at the first five components, r^2_{ncv} 0.959 and predictive r^2 0.855 with steric (22.4%), electrostatic (13.0%), hydrophobic (15.9%), H-bond donor (23.2%) and acceptor (25.4%) field contributions. The 3D contour plots generated from this model are depicted in Figures S8, 8c−e. The graph of actual versus fitted/predicted activities for training/test set molecules is shown in Figure 9b. All five CoMSIA fields contributed significantly to the uPA inhibitory activity of 2-naphthamidines.

1-Isoquinolinylguanidines. Table 5 summarizes the results of CoMSIA PLS analysis for 1-isoquinolinylguanidines. The model generated from the combination of steric and electrostatic fields exhibited better predictions than the CoMFA model with r^2_{cv} 0.752 at five components, r^2_{ncv} 0.976, predictive r^2 0.803 and higher electrostatic field (81.8%) contributions. Inclusion of H-bond donor/acceptor fields resulted in CoMSIA models with comparable internal and decreased external predictive r^2. The CoMSIA model generated using the combination of steric, electrostatic and hydrophobic fields showed the highest predictive r^2 0.855. The combination of all five CoMSIA fields yielded statistically robust model and exhibited r^2_{cv} 0.672 with two components, r^2_{ncv} 0.909, predictive r^2 0.554 with field contribution of steric 25.0%, electrostatic 34.2%, hydrophobic 12.4%, H-bond donor 4.6% and acceptor 23.7%. The 3D contours analyzed for generated model are shown in Figures S9a,b,10b. The graph of actual versus fitted/predicted activities for training/

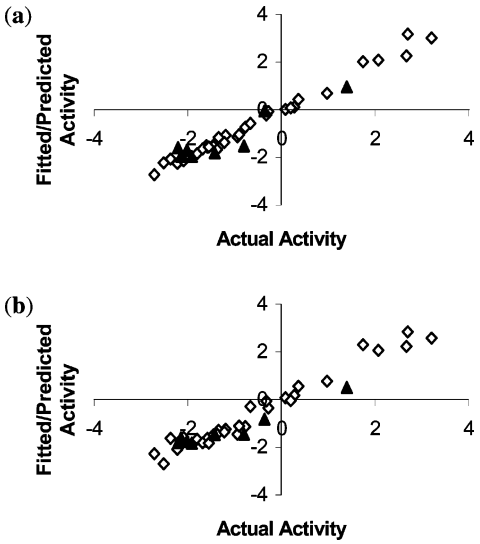

Figure 9. A graph of actual versus fitted/predicted activities for training and test set molecules of 2-naphthamidines. (a) CoMFA. (b) CoMSIA. (◇ training set; ▲ test set).

test set molecules is depicted in Figure 11b. The models derived from the combinations of SEA, SEH, SEDA, SEHD demonstrate considerable predictions with an optimum of twelve, eight, ten and nine components, respectively, and hence can be considered of poor statistical significance. uPA inhibitory activity of 1-isoquinolinylguanidines was found to be contributed significantly by electrostatic, steric, hydrophobic and H-bond acceptor fields.

Predictivity of 3D QSAR Models. The significance and utility of QSAR models is generally checked by predicting the activity of set of molecules, which are not included in model development. A series of 2-naphthamidines as uPA inhibitors with improved pharmacokinetic properties recently reported by Bruncko et al.[34] were used to check the predictive power of the models (Table S6). The 3D structures of the molecules were constructed by modification of X-ray crystal structure obtained from the protein data bank (1owe, 1u6q). After minimization, the lowest energy conformers were aligned on the template molecule (compound **210**) using atom-based rms fitting. The activity of 21 molecules was predicted using CoMFA and CoMSIA models derived for the series of 2-naphthamidines. The CoMFA steric and electrostatic model exhibited r^2_{pred} 0.697, while the CoMSIA model with all five fields showed r^2_{pred} 0.502. The graph of actual versus predicted activities from CoMFA and CoMSIA models for 21 molecules is shown in Figures 12a and 12b, respectively. Statistically significant predictions support the validity of derived models in predicting the activity of newer molecules.

Graphical Interpretation of the CoMFA and CoMSIA Models. The steric contour maps indicate green and yellow contours as sterically favorable and unfavorable areas. Blue and red contours in the electrostatic maps indicate areas where positive and negative charge substitutents favor activity. Hydrophobic, H-bond donor and acceptor contour maps indicate favorable yellow, cyan, magenta contours and disfavorable by white, violet and red contours, respectively. Although the contour maps cannot be used as receptor maps, useful interpretations can be derived. The generated contour maps were mapped on the active site of uPA enzyme (PDB code 1ejn), and fields were analyzed with respect to the amino acid residues of uPA. To aid in visualization, the template molecule in each class of compounds is displayed in the respective figures and the contour maps are discussed with the reference compound.

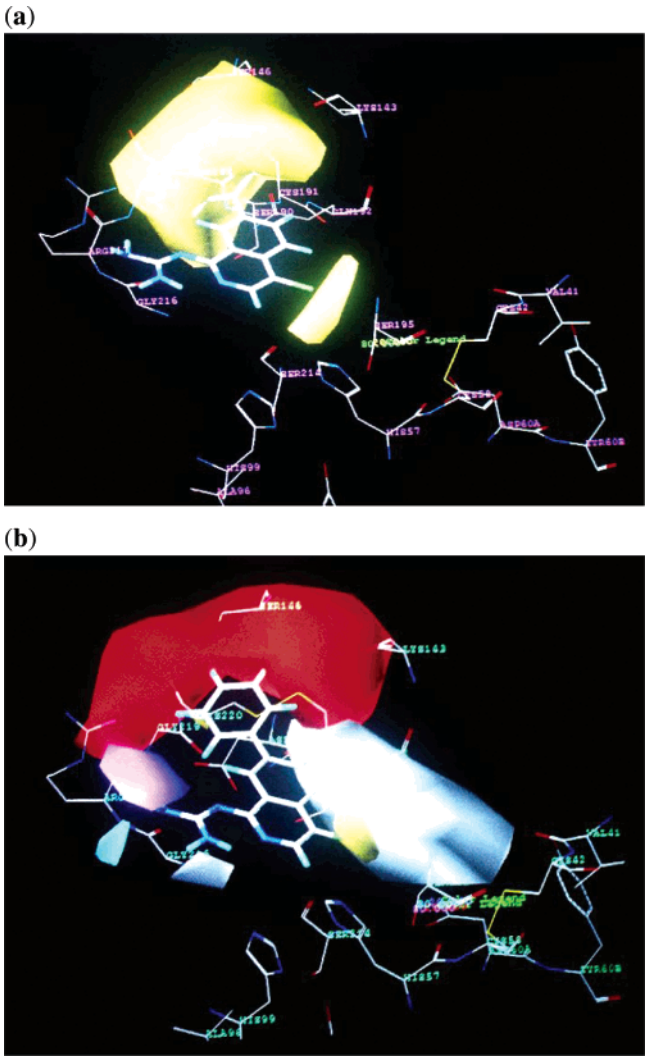

Figure 10. STDDEV*COEFF contour plots for 1-isoquinolynylguanidines superimposed on uPA active sites. (a) CoMFA steric and electrostatic. (b) CoMSIA hydrophobic, H-bond donor and acceptor. The compound **237** in cap and stick is shown.

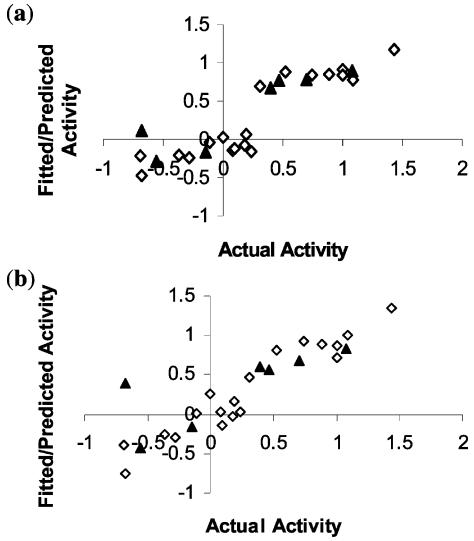

Figure 11. A graph of actual versus fitted/predicted activities for training and test set molecules of 1-isoquinolynylguanidines. (**a**) CoMFA. (**b**) CoMSIA. (◇ training set; ▲ test set).

2-Pyridinylguanidines. Figure 2a corresponds to the CoMFA steric and electrostatic contour maps for 2-pyridinylguanidines

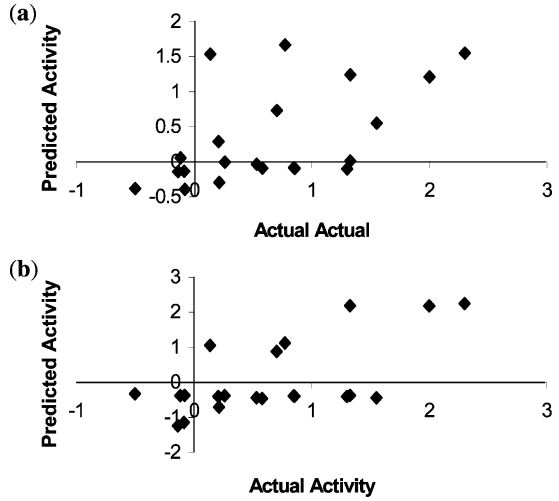

Figure 12. A graph of actual versus predicted activities for test set molecules of 2-naphthamidines. (a) CoMFA. (b) CoMSIA.

with the active molecule (compound **35**). The green contour observed near 5-Cl of pyridinyl and in the vicinity of 2-H of 3-vinylbenzoic acid suggest that steric substitutents in these regions may favor activity (compounds **30**, **34** and **35**), while the disfavored yellow contours surrounding the 3-vinylbenzoic acid and near guanidine restrict the steric substitution indicating decreased biological activity (compounds **3**−**6**, **8** and **9**). In the CoMFA electrostatic map, the large blue contour surrounding 3-vinylbenzoic acid indicates the significance of a positively charged group for biological activity, while small negatively charged favored red contours near 5-Cl specify that the electron rich substituents favor activity. Mapping of CoMFA steric and electrostatic contour plots on uPA active site (Figure S6a) revealed that 3-vinylbenzoic acid was placed in a hydrophobic pocket (S1sub or S1β). The sterically favored green contour in the vicinity of 3-vinylbenzoic acid was placed in this pocket, while the other near 5-Cl was placed near Ser195. The sterically unfavorable yellow contours surrounding 3-vinylbenzoic acid were placed in the periphery of S1 and S1β pocket of uPA. The positively charged favored blue contour surrounding 3-vinylbenzoic acid was placed near Gly219, Cys220, and the small negative charged favored red contour was observed near Ser195 where 5-Cl might have van der Waals contacts.

Figures S6b and S6c displays the CoMSIA steric and electrostatic contour maps, respectively with the active molecule (compound **35**). Sterically unfavorable yellow contours were observed near the guanidine, in the vicinity of pyridinyl and upper part of 3-vinylbenzoic acid, while the sterically favored green polyhedron embedded in the 3-vinylbenzoic acid is almost similar to the CoMFA. The CoMSIA electrostatic contour maps depict large blue polyhedron extending from 3-vinyl to the pyridinyl ring and the red polyhedral observed near 5-Cl.

Figures 2b and 2c display CoMSIA hydrophobic maps superimposed on the uPA active site and the H-bond fields map with compound **35**, respectively. The hydrophobic contour plots connote disfavored large white regions near guanidine, surrounding 3-vinylbenzoic acid, 4-H and 5-Cl, which occupied S1, S1β pockets and the space between Ser195-pyridinyl, where the increased hydrophilic interactions may favor activity. The H-bond donor favorable cyan contours were observed near the guanidinyl NH, whereas the disfavored purple contours appeared near the C-3 vinyl and the guanidinyl NH (compound **7**). Cyan contours were placed in the S1 pocket (Asp189, Gly219) where guanidinyl protons may form water-mediated H-bonding with the Asp189 and Gly219, and the disfavored purple contours were placed near the side chain of Gln192 in the S1 pocket (Figure 2d). The H-bond acceptor contour maps (Figure 2c) show favorable magenta contours in the vicinity of 3-COOH and near the guanidine, while the small red contours are observed near guanidine. 4-Substitution suggests that H-bond acceptor groups to these regions may decrease the activity. H-bond favored magenta contours were placed near Ser146, Lys143 and Gly213. The generated contour maps are in accordance with the findings of Barber et al.,[18] that describe the binding of guanidine in the S1 pocket with Asp189, the 5-halo substituent directing toward catalytic Ser195 and lipophilic 3-substituents exhibiting the highest activity. This is anticipated by the presence of H-bond favorable cyan and magenta contours near guanidine (S1 pocket), a negative charge favored red contour near 5-Cl and a sterically favorable green contour at 3-vinylbenzoic acid (S1β pocket). Therefore, the C-3 and C-5 positions with optimum steric, hydrophilic and H-bonding substituents can be further exploited to improve the activity of 2-pyridinylguanidines.

4-Aminoarylguanidines and 4-Aminobenzamidines. The CoMFA steric and electrostatic contour plots with the template molecule (compound **49**) are shown in Figures 4a. The CoMFA steric contour plot portraying sterically favored green polyhedra surrounding 5′-CH_3 suggests that optimum steric substituents in this region favor activity, whereas sterically disfavored yellow contours were observed near 2-H and other surface of amide carbonyl. The CoMFA electrostatic contour map displays a small red contour embedded in C-4′, while the blue contours in the vicinity of 2-H of phenylguanidine and 5′-CH_3 signify that an increase in activity may be due to low electron density substituents. Naphthyl derivatives, which are placed in the vicinity of green polyhedra, showed improved activity, while the compounds bearing high electron density substituents at C-4′ or C-5′ (compounds **37**, **38**, **41**, **53**, **54** and **57**) were less active. Superimposition of CoMFA steric and electrostatic contour maps on the active site of uPA (Figure S7) displayed green regions near prime-side binding groove defined by Val41, Cys42-Cys58 disulfide bridge and the disfavored yellow regions near Arg217, Gly216, Gln192. A negative charge favored red region embedded in C-4′ was observed near carbonyl of Ser195. CoMSIA steric and electrostatic contour plot portrays large green polyhedra in the vicinity of 5′-CH_3 favors activity while sterically restricted yellow contours were observed in the vicinity of 3′-I (compounds **46** and **62**) almost similar to the CoMFA. In the CoMSIA electrostatic contour plot the blue contours appeared in the vicinity of 2-H, 2′-OH, 5′-CH_3 and negative charge favored small red contour near 3′-I (compounds **48** and **49**).

CoMSIA hydrophobic and H-bond field contour maps are displayed in Figures 4b and 4c, respectively. In the hydrophobic contour map, a favorable large yellow contour displayed in the vicinity of 3′-I was placed in the vicinity of Ser195, while disfavored white contours were observed near 2-H and 3′-I of compound **49** which indicate that optimum lipophilic substituents may enhance or decrease the activity, respectively. An H-bond donor favorable cyan contour was observed in the lower region of guanidine, while unfavorable purple contours were observed on the other planar surface near the carbonyl amide linkage of compound **49**. An H-bond donor favored cyan contour near guanidine was placed in the S1 subsite (near Gly214), while disfavored purple regions were observed near Val213 and Gln192 (Figure 4d). An H-bond acceptor favorable magenta contour was observed near guanidine, and disfavored red contours were observed near guanidine, the carbonyl amide and 5′-CH_3 of compound **49**. A magenta contour was placed near

Ser190, and red contours were observed near Arg217, Cys220, Gln192, Val41 and Cys42 residues of uPA (Figure 4d).

Thiophene-2-carboxamidines. The CoMFA steric and electrostatic contour plots for 4-arylthiazolylthiophene-2-carboxamidines are shown in the Figures 6a and 6b, respectively, with the active molecule (compound **165**). In the CoMFA steric maps (Figure 6a), the large green contours near the 5-SMe of thiophene, the small contour at the C-5 substitution of thiazole and contours surrounding the phenyl ring indicate a region of optimum steric tolerance. Compounds with 5-Me and 5-Et substitutions retained the activity (compounds **76**, **112**, **125** and **126**), whereas unsubstituted or substitution with bulkier groups yielded a decrease in activity (compounds **117** and **124**), thus supporting the significance of 5-SMe in uPA inhibitory activity. Compound **146** with steric substitution of 5-Me extending into the small green contour at C-5 exhibited better activity than compound **147** with a 5-phenyl group. The 2-aminoaryl substituents occupying the large sterically favored green contour extending from 5-SMe displayed better activity (compounds **81**, **84**, **102**−**104**, **107** and **112**) than the unsubstituted counterpart compound **75**. The improved activity of biaryl substituents may be due to their steric flexibility. Improved activity by bulkier groups at C-3 phenyl (compounds **137**−**139**, **161**, **162**, **165**) can be anticipated by the presence of a sterically favored green contour in the vicinity of 3-methylphenyl protons. The CoMFA steric map (Figure 6a) displayed sterically disfavored yellow contours surrounding the green polyhedra placed near 5-SMe (compounds **118**, **119** and **120**), carboxamidine, 5-substituents of thiazole (piperazinyl derivatives compounds **113** and **115**) and near the 4-phenyl ring (compound **151**) that suggest that steric bulk at these regions may not favor activity. The CoMFA contour plot superimposed on the uPA active site (Figure 6c) showed a sterically favored green region near 5-SMe in the vicinity of Ser195, small contours surrounding the phenyl ring in the S1β pocket and another near His57. Yellow regions surrounding green polyhedra were observed near Ser214, Val213, the side chain of His99 and Cys42. Another yellow contour near carboxamidine was observed near Asp189, while contours near 5-substituents were placed in the vicinity of Gly193, Asp195. A sterically forbidden yellow contour near the phenyl ring was placed near Ser146 in the S1β pocket.

The CoMFA electrostatic contour plots (Figure 6b) connote blue contours near carboxamidine, the 5-substituent of thiazole and at the lower surface of thiophene and thiazole of compound **165** and suggest that positively charged groups in these regions may favor activity. Partial positive charges associated with hydrogen atoms bound to carbon can be correlated with the lipophilic interactions. Conversely, negative charge favored regions are portrayed by the red contours near 2-H of the phenyl ring (compounds **140** and **142**) and near the blue contour placed at the lower surface of the thiazole. A blue contour near the carboxamidine was observed in the S1 pocket (Asp189 and Ser190). The other blue contours at the lower surface of thiophene and the 5-substituent of thiazole was observed in the vicinity of Gly193, Asp194 and His57, respectively. A red contour near 2-H of the phenyl ring was placed in the vicinity of the carbonyl of Asp194 and Gly193 (Figure 6c).

2-Naphthamidines. Figures 8a and 8b provide the graphical representation for CoMFA and Figure S8b for CoMSIA models of 2-naphthamidines using steric and electrostatic fields with the active molecule (compound **210**). The CoMFA steric contour plot shows a large green polyhedron embedded in the pyrimidine ring wherein high steric tolerance at C-8 of naphthamidine may enhance the activity. Conversely, large sterically unfavorable yellow contours are observed surrounding the methylamino group and in the vicinity of 7-H of naphthamidine of compound **210**. CoMFA contour map superimposed on the uPA active site (Figure S8a) displayed sterically forbidden yellow regions around the methylamino group in the vicinity of the Cys42-Cys58 disulfide bridge, Val41, Asp60A and another contour in the vicinity of 7-H near Gln192. Compounds with 7-OMe extending into the yellow region near Gln192 displayed less activity (compounds **195**−**200**). Similarly, steric substituents extending into yellow contours around methylamino also displayed decreased activity (compounds **174**, **175**, **187**−**194**). CoMFA electrostatic contour plots displayed a positively charged favored large blue contour at the upper surface of naphthamidine and small contours near the pyrimidine ring and methylamine of compound **210**. Negative charged favored red contours were observed near pyrimidine ring, embedded in 6-carbonylamide linkage and in the vicinity of 3-H of the phenyl. The CoMSIA steric contour maps were almost similar to CoMFA, while the CoMSIA electrostatic contour plot portrays blue contours in the vicinity of upper surface of naphthamidine and red contour embedded in the phenyl ring (Figure S8b). CoMSIA hydrophobic, H-bond field contour maps are displaced in Figures 8c−e. The CoMSIA hydrophobic contour map displays favorable yellow contours embedded in the upper surface of pyrimidine, near C-2 of naphthamidine and the phenyl ring of compound **210**, where increased hydrophobic interactions support biological activity, while the unfavorable white contours in the vicinity of C-8 naphthamidine near C-3 phenyl suggests that hydrophilic groups in these regions may favor activity. Yellow regions at the upper surface of the pyrimidine occupied the lipophilic S1β subsite, while the yellow contour near the phenyl ring may have π-stacking interactions with imidazole of His57 and van der Waals interactions with the side chain of Val41, Cys42-Cys58 disulfide ring. The unfavorable white contours in the vicinity of naphthamidine observed in the vicinity of Gln192 (S1 pocket). The CoMSIA H-bond donor map displayed a favorable large cyan contour observed near 8-NH, whereas purple contours were observed near amide NH, C-3 phenyl substitutions. An H-bond favored region was observed in the vicinity of Gln192 in the S1 subsite, and disfavored regions were observed near the carbonyl of Ser214 and Cys58, His57 carboxylate. The H-bond acceptor map showed favorable magenta contours near the pyrimidine ring and 8-NH naphthamidine. Conversely, the unfavorable red contours were observed near 2-carboxamidine, in the vicinity of amide carbonyl and phenyl ring of compound **210**. Magenta regions observed near Cys191, Gln192 and red contours near Gly216, Arg217, in the vicinity of Gln192, Ser195, Cys42 and Val41. It is evident from the literature that amide NH is involved in a water-mediated H-bond to Ser214, the amide carbonyl seem to interact with Gln192 which in turn is H-bonded through its amide carbonyl to Lys143, and the aminomethyl forms a salt bridge interaction with Asp60A carbonate and the charged amino group.[21b]

1-Isoquinolinylguanidine. The graphical representation for the CoMFA model superimposed on uPA active sites and CoMSIA model from steric and electrostatic fields with reference compound **237** is depicted in Figures 10a and S9a,b, respectively. The CoMFA steric contour map displayed sterically unfavorable yellow contours engulfing the 7-phenyl and near 4-Cl of isoquinolinylguanidine. The electrostatic contour map showed prominent large blue contours near the upper surface of the guanidine moiety and small red contours near the carboxyl group, suggesting that the increase in activity may be due to the presence of an electron rich substitutent group (compounds

237, **238**). The S1β subsite of the enzyme was occupied by a sterically disfavored yellow region engulfing the 7-phenyl, restricting the larger substituents at this position, and another yellow contour near 4-Cl was placed near Ser195. A blue polyhedron was observed in the vicinity of the main chain atoms of Arg217, Gly219 at the rim of the S1 site, and the red contours were placed near Lys143, Cys91. The CoMSIA steric contour map displayed sterically unfavorable yellow contours engulfing the 7-phenyl similar to CoMFA. The electrostatic contour map showed large blue contours embedded in the 5-H of isoquinoline ring and near the 4-H of 7-phenyl ring, suggesting that low electron density substituents at these positions may enhance activity; conversely, red contours near the 7-phenyl ring suggest that high electron density substituents may favor activity.

Figure 10b depicts the CoMSIA hydrophobic, H-bond donor and acceptor field contour maps superimposed on the uPA active site. The CoMSIA hydrophobic contour map displayed a disfavored large white contour in the vicinity of the 5,6-H of the isoquinoline ring and the guanidine NH, while favored yellow contours in the vicinity of 4-Cl of the isoquinolinyl suggests that increased hydrophobic interactions disfavor/favor activity, respectively. The superimposed map displayed hydrophobic disfavored white regions in the S1 pocket (Gly216), in the vicinity of Cys191, Gln192, Gly193, Asp194, Ser195 and the favored yellow region near Ser195. The H-bond donor contour map displayed a favorable cyan contour near the guanidine and an unfavorable purple contour surrounding guanidine. The superimposed H-bond contour plot showed purple regions near guanidine placed near Asp189, Gly219 in the S1 subsite, and the disfavored large red contour which forms a cavity around the 7-phenyl ring was placed at the rim of the S1β subsite (Ser146, Lys143). The electrostatic contour map developed is consistent with the SAR results where methyl substitution at 4-position (compound **212**) is tolerated, while halosubstitution (Cl or Br) is generally preferred (compounds **213** and **214**).[22] Increase in activity by the low electron density substituents at the 5-position of isoquinoline can be anticipated by the presence of a positive charge favorable blue contour. This is supported by a decrease in potency by 5-substituents (compounds **215**−**218**). Further, optimum lipophilic substituents at C-5, C-6 positions and hydrophobic substituents at the C-4 position of isoquinoline may enhance the activity.

Comparison of 3D QSAR Models in Subsites of Serine Proteases. Trypsin-like serine proteases are characterized by the presence of amino acid residues at position 190 at the S1 subsite. uPA, trypsin and tryptase possess a serine residue, whereas tPA, thrombin and factor Xa possesses an alanine residue at 190. Ser190 forms an additional H-bond with S1-bound amidine inhibitors, which impart an increased affinity of amidine inhibitors toward uPA over that of alanine counterparts. The protease−amidine complexes showed significant differences in relative orientation of bound inhibitors, their degree of planarity, depths in the S1 pocket, variability in their relative positions, conformation of Asp189 and its position and H-bonding interactions of the water cobound at S1.[24g] The S1 site of uPA is composed of a Cys191-Cys220 disulfide bridge and main chain atoms of Ser214, Cys220, Gln192, side chains of Val213, Asp189, Ser190, Ser195 and Gly218; hence both hydrophobic and hydrophilic contacts occur at S1. The selectivity of indole/benzoimidazole-2-carboxamidines toward uPA was achieved by introduction of the halo substituent near 2-carboxamidine, which displaces the water.[17a] Presence of H-bond favorable contours (cyan/magenta) near guanidine/carboxamidine in the S1 pocket signifies the importance of the basic functional groups in affinity of the these inhibitors toward uPA.

The S1β pocket at the proximity of the primary S1 site is composed of a Cys191-Cys220 disulfide bridge, residues Gly218, Ser146 and the side chain of Lys143. Molecular superimposition of data set on uPA active sites revealed that the 3-vinylbenzoic acid substituent of 2-pyridinylguanidines, 5-substituents of 4-(thiazol-2-yl)-thiophene-2-carboxamidines, 8-substituents of 2-naphthamidines, and the 7-substituent of 1-isoquinolinylguanidines occupy the S1β pocket of uPA. 2-Pyridinylguanidines and 1-isoquinolinylguanidines showed close similarity in their structures. 3-Vinyl-linked substituents of 2-pyridinylguanidines and the 7-substituent of 1-isoquinolinylguanidines occupied the S1β pocket, while C-5 and C-4 substituents of 2-pyridinylguanidines and 1-isoquinolinylguanidines directed toward catalytic Ser195. The 3D QSAR models developed for both series showed comparable contours characterized by sterically favored green contours surrounded by disfavored yellow contours in the S1β subsite, negative charged favored small red contours near Ser195, lipophilic favored large white regions extending toward Ser195, and H-bond donor favored cyan contours near guanidine in the S1 subsite of uPA. Similarly, 8-substituents of 2-naphthamidines occupied the S1β subsite, where the 3D contour maps displayed steric, high electron density, hydrophobic, lipophilic and H-bond field favored regions.

A hydrophobic small dimple (S2 subsite) of uPA defined by an imidazole side chain of His57 and Lys92 is relatively small due to His99; hence the hydrophobic contact with π-stacking interactions occurs at the S2 subsite. 4-Arylcarbonylamide substituents of 4-aminoarylguanidines/benzamidines, 2-substituents of 4-(thiazol-2-yl)-thiophene-2-carboxamidines and C-7 substituents of 2-naphthamidines oriented toward the S2 subsite. Extending out in the opposite direction from the S2 subsite is a very broad, shallow prime-side protein binding group immediately defined by Tyr60B, Gln192 with the floor of the groove defined by Val41 and the Cys42-Cys58 disulfide bond. 7-Aryl substituents of 2-naphthamidines may have interactions with this subsite due to the 7-carbonylamide linkage. Overall, the 3D QSAR models developed for various chemical series showed comparable similarities in the binding sites of uPA.

The contour maps generated for the series of 2-naphthamidines were superimposed on the active sites of other serine proteases trypsin (1o3i), thrombin (1o3g) and fXa (1lqe). The CoMFA steric and electrostatic maps superimposed on uPA and other serine proteases are displayed in Figure S10, whereas CoMSIA hydrophobic and H-bond maps are depicted in Figures S11 and S12, respectively. Subtle differences in amino acid residues in the binding pockets of serine proteases and their interactions with inhibitors may be crucial in achieving selectivity. The prime-side protein binding pocket of uPA showed sterically disfavored yellow contours in the vicinity of Val41 and near Asp60A, Tyr60B, a positive charge favored blue contour, a hydrophobic favored yellow contours near Val41 and H-bond acceptor disfavored red contours near Val41 favoring hydrophobic and van der Waals interactions. Val41 of uPA is substituted by aromatic Phe41 in trypsin and fXa and by Leu41 in thrombin; thus increased hydrophobic interactions are preferred for improved activity of trypsin and fXa. H-bond donor disfavored purple contours and hydrophobic favored yellow contours observed in the small hydrophobic dimple (S2 subsite) of uPA favored hydrophobic interactions, whereas the large S2 subsite in other serine proteases is accessible for hydrophobic interactions due to substitution of His99 by Leu99. In the S1β

pocket, Asn143 substitutes Lys143 in trypsin, thrombin and fXa, and Ser146 is replaced with Glu146 in thrombin, which may be responsible for different binding affinities. The increased affinity for trypsin in the direct linked 8-substituted naphthamidines alkylsulfonylfuran (compounds **205**, **206**), methylsulfonylpyrazole (compound **200**) and ethylthiofuran (compound **204**) may be due to the interactions with Asn143. Steric, lipophilic, negative charged, H-bond field favored contours were observed in the S1β pocket. Overall the superimposed maps displayed some degree of variation in their placement in the enzymes active sites.

Conclusions

3D QSAR studies yielded stable and statistically significant predictive models indicated by the moderate to high cross-correlation coefficients. A high bootstrapped r^2 value and a small standard deviation indicate that a similar relationship exists in all compounds of the series used in the study. The CoMFA models generated from the atom-based rms fit method exhibited comparatively better models than the rmsd-based database fitting method. The CoMFA steric and electrostatic field contributions in all chemical series revealed relatively higher contributions of steric fields. Further, inclusion of an additional descriptor, ClogP, in CoMFA analysis yielded comparable models with CoMFA steric and electrostatic field. The higher contribution of ClogP was observed for 2-pyridinylguanidines (20%) as compared to other chemical series (0.8−5.4%).

The comparison of CoMFA and CoMSIA models obtained using steric and electrostatic fields suggests that CoMFA yielded relatively improved models for 2-pyridinylguanidines, 4-aminoarylguanidines/4-aminobenzamidines and thiophene-2-carboxamidines. CoMSIA yielded fairly improved models for 2-naphthamidines and 1-isoquinolinylguanidines and statistically insignificant models for thiophene-2-carboxamidines. Overall, CoMSIA yielded comparable models for 4-aminoarylguanidines/4-aminobenzamidines, 2-naphthamidines and 1-isoquinolinylguanidines with CoMFA, highlighting the significance of hydrophobic and H-bond fields toward uPA inhibitory activity of these molecules, while the CoMSIA method yielded statistically poor models for thiophene-2-carboxamidines.

The CoMSIA steric and electrostatic field maps are in accordance with field distribution of CoMFA maps and consistent with structure−activity relationships. The comparison of 3D QSAR models with the active site of uPA revealed the interactions of amino acid residues with the substructures of molecules with steric, electrostatic, hydrophobic, H-bond fields around them.

In the present studies, we have identified the significance of various structural elements binding at different subsites, which may be combined to improve overall activity. It was observed that 2-naphthamidines exhibited the highest activity, which may be due to the combined interactions of the substituents in the S1, S1β, S2 and proximal lipophilic subsites, as evident from the contour maps superimposed on uPA active sites. The significant predictive ability of 3D QSAR models observed for the external test molecules supports that the derived models can be used for the design of novel inhibitors. Overall, the present 3D QSAR study investigates the indispensable structural features of the different chemical classes of molecules which can be exploited for the structural modifications of these lead molecules in order to achieve improved selective uPA inhibitory activity.

Acknowledgment. We thank Dr. F. V. Manvi, Principal, Prof. A. D. Taranalli, Vice-Principal, KLES's College of Pharmacy, Belgaum, India, for providing necessary facilities, and Dr. Santosh Kulkarni for useful suggestions. B.A.B. is thankful to Human Resource Development Group, Council for Scientific and Industrial Research, New Delhi, India, for the award of Senior Research Fellowship [8/470(1)/2001-EMR-I]. We acknowledge All India Council for Technical Education, New Delhi, India, for the financial support [File No. 8018/RDII/BOR/TAP (397)/99-2000].

Supporting Information Available: Structures and biological activity of the data sets are described in Tables S1−S5, and the views of the aligned molecules by the atom-based rms method superimposed on crystal structures are depicted in Figures S1−S5. CoMFA steric and electrostatic STDDEV*COEFF contour plots superimposed on uPA active sites for 2-pyridinylguanidines, 4-aminoarylguanidines/benzamidines and 2-naphthamidines are displayed in Figures S6a, S7 and S8a, respectively. CoMSIA steric and electrostatic STDDEV*COEFF contour plots for 2-pyridinylguanidines, 2-naphthamidines and 1-isoquinolinylguanidines are displayed in Figures S6b,c, S8 and S9a,b, respectively. STDDEV*-COEFF contour plots for 2-naphthamidines superimposed on trypsin, thrombin and fXa are displayed in Figures S10a−c (CoMFA steric and electrostatic), S11a−c (CoMSIA hydrophobic) and S11a−c (CoMSIA H-bond fields). This material is available free of charge via the Internet at http://pubs.acs.org.

References

(1) (a) Dano, K.; Romer, J.; Nielsen, B. S.; Bjorn, S.; Pyke, C.; Rygaard, J.; Lund, L. R. Cancer invasion and tissue remodeling: cooperation of protease systems and cell types. *APMIS* **1999**, *107*, 120−127. (b) Jan, W. A. S.; van der Pluijm, G.; Hans, A. R.; Lowik, C. W. G. M.; Hans, M.; Bernard, M. G. Degradation of extracellular matrix by metastatic follicular thyroid carcinoma. *Thyroid* **1999**, *9*, 913−919.

(2) Dano, K.; Andreasen, P. A.; Grondahl-Hansen, J.; Kristensen, P.; Nielsen, L. S.; Skriver, L. Plasminogen activators, tissue degradation and cancer. *Adv. Cancer Res.* **1985**, *44*, 139−266.

(3) (a) Saksela, O. Plasminogen activation and regulation of pericellular proteolysis. *Biochim. Biophys. Acta* **1985**, *823*, 35−65. (b) Testa, J. E.; Qiugley, J. P. The role of urokinase-type plasminogen activator in aggressive tumor cell behaviour. *Cancer Metast. Rev.* **1990**, *9*, 353−367. (c) Gunzler, W. A.; Steffens, G. J.; Otting, F.; Kim, S. M. A.; Frankus, E.; Flohe, L. The primary structure of high molecular mass urokinase from human urine. *Hoppe. Seyler. Z. Physiol. Chem.* **1982**, *363*, 1155−1165.

(4) Mignatti, P.; Robbins, E.; Rifkin, D. B. Tumor invasion through the human amniotic membrane: requirement for a proteinase cascade. *Cell* **1986**, *47*, 487−498.

(5) (a) Werb, Z.; Mainardi, C. L.; Vater, C. A.; Harris, E. D., Jr. Endogenous activation of latent collagenase by rheumatoid synovial cells. Evidence for a role of plasminogen activator. *New Engl. J. Med.* **1977**, *296*, 1017−1023. (b) Paranjpe, M.; Engel, L.; Young, N.; Liotta, L. A. Activation of human breast carcinoma collagenase through plasminogen activator. *Life Sci.* **1980**, *26*, 1223−1231.

(6) (a) Cook, A. D.; Braine, E. L.; Campbell, I. K.; Hamilton, J. A. Differing roles for urokinase and tissue-type plasminogen activator in collagen-induced arthritis. *Am. J. Pathol.* **2002**, *160*, 917−926. (b) Busso, N.; Pleclat, V.; So, A.; Sappino, A.-P. Plasminogen activation in synovial tissues: Differences between normal, osteoarthritis, and rheumatoid arthritis joints. *Ann. Rheum. Dis.* **1997**, *56*, 550−557.

(7) (a) Noda-Heiny, H.; Daughety, A.; Sobel, B. E. Augmented urokinase receptor expression in atheroma. *Arterioscler. Thromb. Vasc. Biol.* **1995**, *15*, 37−43. (b) Carmeliet, P.; Moons, L.; Lijnen, R.; Baes, M.; Lemaitre, V.; Tipping, P.; Drew, A.; Eeckhout, Y.; Shapiro, S.; Lipu, F.; Collen, D. Urokinase-generated plasmin activates matrix metalloproteinases during aneurism formation. *Nature Genet.* **1997**, *17*, 439−444. (c) Falkenberg, M.; Giglio, D.; Bjornheden, T.; Nygren, H.; Risberg, B. Urokinase plasminogen activator colocalizes with CD25+ cells in atherosclerotic vessels. *J. Vasc. Res.* **1998**, *35*, 318−324. (d) Preissner, K. T.; Kanse, S. M.; Chavakis, T.; May, A. E. The dual role of the urokinse receptor system in pericellular proteolysis and cell adhesion. Implications for cardiovascular function. *Basic Res. Cardiol.* **1999**, *94*, 315−321.

(8) Kanse, S. M.; Benzakour, O.; Kanthou, C.; Kost, C.; Lijnen, H. R.; Preissner, K. T. Induction of vascular SMC proliferation by urokinase indicates novel mechanism of action in vasoproliferative disorders. *Arteriosler. Thromb. Vasc. Biol.* **1997**, *17*, 2848−2855.

(9) (a) Rabbani, S. A.; Xing, R. H. Role of urokinase (uPA) and its receptor (uPAR) in invasive and metastasis of hormone-dependent malignancies. *J. Int. Oncol.* **1998**, *12*, 911−920. (b) Bell, W. R. The fibronolytic system in neoplasia. *Sem. Thromb. Hemost.* **1996**, *22*, 459−478. (c) Blasi, F. The urokinase receptor, A cell surface, regulated chemokine. *APMIS* **1999**, *107*, 96−101.

(10) (a) Andersen, P. A.; Kjoller, L.; Christensen, L.; Duffy, M. J. The urokinse-type plasminogen activator system in cancer metastasis: A review. *Int. J. Cancer* **1997**, *72*, 1−22. (b) Achbarou, A.; Kaiser, S.; Tremblay, G.; Sainte-Marie, L.; Brodt, P.; Goltzman, D.; Rabbani, S. A. *Cancer Res.* **1994**, *54*, 2372−2377. (c) Duffy, M. J. Urokinse-type plasminogen activator: a potent marker of metastatic potential in human cancers. *Biochem. Soc. Trans.* **2002**, *30*, 207−210.

(11) (a) Pappot, H.; Brunner, N. The plasminogen activation system and its role in lung cancer. a review. *Lung Cancer* **1995**, *12*, 1−12. (b) Schmitt, M.; Wilhelm, O. G.; Reuning, U.; Kruger, A.; Harbeck, N.; Lengyel, E.; Graeff, H.; Gansbacher, B.; Kessler, H.; Burgle, M.; Sturzebecher, J.; Sperl, S.; Magdolen, V. The urokinase plasminogen activator system as a novel target for tumor therapy. *Fibrinol. Proteol.* **2000**, *14*, 114−132. (c) Tsatas, D.; Kaye, A. H. The role of the plasminogen activation cascade in glioma cell invasion: a review. *J. Clin. Neurosci.* **2003**, *10*, 139−145.

(12) Collen, D.; Lijnen, H. R. Basic and clinical aspects of fibrinolysis and thrombolysis. *Blood* **1991**, *78*, 3114−3124.

(13) (a) Sturzebecher, J.; Markwardt, F. Synthetizche inhibitorren der serineproteinasen. *Pharmazie* **1978**, *33*, 599−602. (b) Tidwell, R. R.; Geratz, J. D.; Dubovi, E. J. Aromatic amidines. Comparison of their ability to block respiratory syncytial virus induced cell fusion and to inhibit plasmin, urokinase, thrombin, and trypsin. *J. Med. Chem.* **1983**, *26*, 294−298.

(14) (a) Yang, H.; Henkin, J. Selective inhibition of urokinase by substituted phenylguanidines: Quantitative structure−activity relationship analyses. *J. Med. Chem.* **1990**, *33*, 2956−2961. (b) Yang, H.; Henkin, J. Competitative inhibitors of human urokinase. *Fibrinolysis* **1992**, *6*, 31−34.

(15) Vassalli, J.-D.; Belin, D. Amiloride selectivity inhibits the urokinase-type plasminogen activator. *FEBS Lett.* **1987**, *214*, 187−191.

(16) (a) Towle, M. J.; Lee, A.; Maduakor, E. C.; Schwartz, C. E.; Bridges, A. J.; Littlefield, B. A. Inhibition of urokinase by 4-substituted benzo(*b*)thiophene-2-carboxamidines: An important new class of selective synthetic urokinase inhibitor. *Cancer Res.* **1993**, *53*, 3553−2559. (b) Bridges, A. J.; Lee, A.; Schwartz, C. E.; Towle, M. J.; Littlefield, B. A. The synthesis of three 4-substituted benzo[*b*]thiophene-2-carboxamidines as potent and selective inhibitors of urokinase. *Bioorg. Med. Chem.* **1993**, *1*, 403−410.

(17) (a) Mackman, R. L.; Katz, B. A.; Breitenbucher, J. G.; Hui, H. C.; Verner, E.; Luong, C.; Liu, L.; Sprengeler, P. A. Exploiting subsite S1 of trypsin-like serine proteases for selectivity: Potent and selective inhibitors of urokinase-type plasminogen activator. *J. Med. Chem.* **2001**, *44*, 3856−3871. (b) Verner, E.; Katz, B. A.; Spencer, J. R.; Allen, D.; Hataye, J.; Hruzewicz, W.; Hui, H. C.; Kolesnikov, A.; Li, Y.; Luong, C.; Martelli, A.; Radika, K.; Rai, R.; She, M.; Shrader, W.; Sprengeler, P. A.; Trapp, S.; Wang, J.; Young, W. B.; Mackman, R. L. Development of serine protease inhibitors displaying a multicentered short (<2.3 Å) hydrogen bond binding mode: Inhibitors of urokinase-type plasminogen activator and factor Xa. *J. Med. Chem.* **2001**, *44*, 2753−2771. (c) Mackman, R. L.; Hui, H. C.; Breitenbucher, J. G.; Katz, B. A.; Luong, C.; Martelli, A.; McGee, D.; Radika, K.; Sendzik, M.; Spencer, J. R.; Sprengeler, P. A.; Tario, J.; Verner, E.; Wang, J. 2-(2-Hydroxy-3-alkoxyphenyl)-1-*H*-benzimidazole-5-carboxamidine derivatives as potent and selective urokinase-type plasminogen activator inhibitors. *Bioorg. Med. Chem. Lett.* **2002**, *12*, 2019−2022.

(18) (a) Barber, C. G.; Dickinson, R. P.; Horne, V. A. Selective urokinase-type plasminogen activator (uPA) inhibitors. Part 1: 2-Pyridinylguanidines. *Bioorg. Med. Chem. Lett.* **2002**, *12*, 181−184. (b) Barber, C. G.; Dickinson, R. P. Selective urokinase-type plasminogen activator (uPA) inhibitors. Part 2: (3-Substituted-5-halo-2-Pyridinyl)-guanidines. *Bioorg. Med. Chem. Lett.* **2002**, *12*, 185−187.

(19) Spencer, J. R.; McGee, D.; Allen, D.; Katz, B. A.; Luong, C.; Sendzik, M.; Squires, N.; Mackman, R. L. 4-Amimoarylguanidine and 4-amimobenzamidine derivatives as potent and selective urokinase-type plasminogen activator inhibitors. *Bioorg. Med. Chem. Lett.* **2002**, *12*, 2023−2026.

(20) (a) Subasinghe, N. L.; Illig, C.; Hoffman, J.; Rudolph, M. J.; Wilson, K. J.; Soll, R.; Randle, T.; Green, D.; Lewandowski, F.; Zhang, M.; Bone, R.; Spurlino, J.; DesJarlais, R.; Deckman, I.; Molloy, C. J.; Manthaey, C.; Zhou, Z.; Sharp, C.; Maguire, D.; Crysler, C.; Grasberger, B. Structure-based design, synthesis and SAR of a novel series of thiopheneamidine urokinase plasminogen activator inhibitors. *Bioorg. Med. Chem. Lett.* **2001**, *11*, 1379−1382. (b) Wilson, K. J.; Illig, C. R.; Subasinghe, N. L.; Hoffman, J. B.; Rudolph, M. J.; Soll, R.; Molloy, C. J.; Bone, R.; Green, D.; Randall, T.; Zhang, M.; Lewandowski, F. A.; Zhou, Z.; Sharp, C.; Maguire, D.; Grasberger, B.; DesJarlais, R.; Spurlino, J. Synthesis of thiophene-2-carboxamidines containing 2-aminothiazoles and their biological evaluation as urokinase inhibitors. *Bioorg. Med. Chem. Lett.* **2001**, *11*, 915−918. (c) Rudolph, M. J.; Illig, C. R.; Subasinghe, N. L.; Wilson, K. J.; Hoffman, J. B.; Randle, T.; Green, D.; Molloy, C. J.; Soll, R. M.; Lewandowski, F.; Zhang, M.; Bone, R.; Spurlino, J. C.; Deckman, I. C.; Manthey, C.; Sharp, C.; Maguire, D.; Grasberger, B. L.; DesJarlais, R. eL.; Zhou, Z. Design and synthesis of 4,5-disubstituted-thiophene-2-amidines as potent urokinase inhibitors. *Bioorg. Med. Chem. Lett.* **2002**, *12*, 491−495.

(21) (a) Wendt, M. D.; Geyer, A.; McClellan, W. J.; Rockway, T. W.; Weitzberg, M.; Zhao, X.; Mantei, R.; Stewart, K.; Nienaber, V.; Klinghofer, V.; Giranda, V. L. Interaction with the S1β-pocket of urokinase: 8-heterocycle substituted and 6,8-disubstituted 2-naphthamidine urokinase inhibitors. *Bioorg. Med. Chem. Lett.* **2004**, *14*, 3063−3068. (b) Wendt, M. D.; Rockway, T. W.; Geyer, A.; McClellan, W. J.; Weitzberg, M.; Zhao, X.; Mantei, R.; Nienaber, V. L.; Stewart, K.; Klinghofer, V.; Giranda, V. L. Identification of novel binding interactions in the development of potent, selective 2-naphthamidine inhibitors of urokinase. Synthesis, structural analysis and SAR of *N*-phenyl amide 6-substitution. *J. Med. Chem.* **2004**, *47*, 303−324.

(22) Barber, C. G.; Dickinson, R. P.; Fish, P. V. Selective urokinase-type plasminogen activator (uPA) inhibitors. Part 3: 1-Isoquinolinylguanidines. *Bioorg. Med. Chem. Lett.* **2004**, *14*, 3227−3230.

(23) Hajduk, P. J.; Boyd, S.; Nettesheim. D.; Nienaber, V. L.; Severin, J.; Smith, R.; Davidson, D.; Rockway, T.; Fesik, S. W. Identification of novel inhibitors of urokinase via NMR-based screening. *J. Med. Chem.* **2000**, *43*, 3862−3866.

(24) (a) Nienaber, V. L.; Davidson, D.; Edalji, R.; Girande, V. L.; Klinghofer, V.; Henkin, J.; Magdalinos, P.; Mantei, R.; Merrick, S.; Severin, J. M.; Smith, R. A.; Stewart, K.; Walter, K.; Wang, J.; Wendt, M.; Weitzberg, M.; Zhao, X.; Rockway, T. Structure-directed discovery of potent nonpeptidic inhibitors of human urokinase that access a novel binding subsite. *Structure* **2000**, *8*, 553−563. (b) Zeslawska, E.; Schweinitz, A.; Karcher, A.; Sondermann, P.; Sperl, S.; Sturzebecher, J.; Jacob, U. Crystals of Urokinase type plasminogen activator variant βc-uPA in complex with small molecule inhibitor open the way towards structure based drug design. *J. Mol. Biol.* **2000**, *301*, 465−475. (c) Sperl, S.; Jacob, U.; Arroyo De Prada, N.; Stuerzebecher, J.; Wilhelm, O. G.; Bode, W.; Magdolen, V.; Huber, R.; Moroder, L. (4-Aminomethyl)phenylguanidine derivatives as non-peptidic highly selective inhibitors of human urokinase. *Proc. Natl. Acad. Sci. U.S.A.* **2000**, *97*, 5113−5118. (d) Zeslawska, E.; Schweinitz, A.; Karcher, A.; Sondermann, P.; Sperl, S.; Sturzebecher, J.; Jacob, U. Crystals of the urokinase type plasminogen activator variant Bc-uPA in complex with small molecule inhibitors open the way towards structure-based drug design. *J. Mol. Biol.* **2000**, *301*, 465−475. (e) Katz, B. A.; Elrod, K.; Rice, M.; Mackman, R. L.; Sprengeler, P. A.; Spencer, J. R.; Hatayte, J.; Janc, J.; Link, J.; Litvak, J.; Rai, R.; Rice, K.; Sideris, S.; Verner, E.; Young, W. A novel serine protease inhibition motif involving a multi-centered short hydrogen bonding network at the active site. *J. Mol. Biol.* **2001**, *307*, 1451−1488. (f) Nienaber, V. L.; Wang, J.; Davidson, D.; Henkin, J. Re-engineering of human urokinase provides a system for structure based drug design at high resolution and reveals a novel structural subsite. *J. Biol. Chem.* **2000**, *275*, 7239−7248. (g) Katz, B. A.; Mackman, R.; Luong, C.; Radika, K.; Martelli, A.; Sprengeler, P. A.; Wang, J.; Chan, H.; Wong, L. Structural basis for the selectivity of a small molecule, S1-binding submicromolar inhibitor of of urokinase-type plasminogen activator. *Chem. Biol.* **2000**, *7*, 299−312. (h) Katz, B. A.; Sprengeler, P. A.; Luong, C.; Verner, E.; Elrod, K.; Kirtley, M.; Janc, J.; Spencer, J. R.; Breitenbucher, J. G.; Hui, H.; Mcgee, D.; Allen, D.; Martelli, A.; Mackman, R. L. Engineering inhibitors highly selective for the S1 sites of Ser190 trypsin-like serine protease drug targets. *Chem. Biol.* **2001**, *8*, 1107−1121. (i) Klinghofer, V.; Stewart, K.; McGonigal, T.; Smith, R.; Sarthy, A.; Nienaber, V. L.; Butler, C.; Dorwin, S.; Richardson, P.; Weitzberg, M.; Wendt, M.; Rockway, T.; Zhao, X.; Hulkower, K. L.; Girande, V. L. Species specificity of amidine-based urokinase inhibitors. *Biochemistry* **2001**, *40*, 9125−9131. (j) Katz, B. A.; Elrod, K.; Verner, E.; Mackman, R. L.; Luong, C.; Shrader, W. D.; Sendzik, M.; Spencer. J. R.; Sprengeler, P. A.; Kolesnikow, A.; Tai, V. W.; Hui, H. C.; Breitenbucher, J. G.; Allen, D.; Janc, J. W. Elaborate manifold of short hydrogen bond arrays mediating binding of active site-directed serine protease inhibitors. *J. Mol. Biol.* **2003**, *329*, 93−120. (k) Katz, B. A.; Luong, C.; Ho, J. D.; Somoza, J. R.; Gjerstad, E.; Tang, J.; Williams, S. R.; Verner, E.; Mackman, R. L.; Young, W. B.; Sprengeler, P. A.; Chan, H.; Mortara, K.; Janc, J. W.; Mcgrath, M. E. Dissecting and designing inhibitor selectivity determinants at the S1 site using an artificial Ala190 protease (Ala190 uPA). *J. Mol. Biol.* **2004**, *344*, 527−545.

(25) (a) Bhongade, B. A.; Gadad, A. K. 3D-QSAR CoMFA/CoMSIA studies on urokinase plasminogen activator (uPA) inhibitors: a strategic design in novel anticancer agents. *Bioorg. Med. Chem.* **2004**, *12*, 2797−2805. (b) Bhongade, B. A.; Gouripur, V. V.; Gadad, A. K. 3D-QSAR CoMFA studies on trypsin-like serine protease inhibitors: a comparative selectivity analysis. *Bioorg. Med. Chem.* **2005**, *13*, 2773−2782.

(26) Cramer, R. D., III.; Patterson, D. E.; Bunce, J. D. Comparative molecular field analysis (CoMFA): 1. Effect of shape on binding of steroids to carrier proteins. *J. Am. Chem. Soc.* **1988**, *110*, 5959−5967.

(27) Klebe, G.; Abraham, U.; Mietzner, T. Molecular similarity indices in a comparative analysis (CoMSIA) of drug molecules to correlate and predict their biological activity. *J. Med. Chem.* **1994**, *37*, 4130−4146.

(28) Leo, A. J. Calculating log P_{oct} from structures. *Chem. Rev.* **1993**, *93*, 1281−1306.

(29) *SYBYL Molecular Modeling Software*, version 6.7; Tripos Inc., St. Louis, MO, 2000.

(30) Stewart, J. J. MOPAC: A semiempirical molecular orbital program. *J. Comput.-Aided Mol. Des.* **1990**, *4*, 1−105.

(31) Dewar, M. J. S.; Zoebisch, E. G.; Healy, E. F.; Stewart, J. J. P. AM1: A new general purpose quantum mechanical molecular model. *J. Am. Chem. Soc.* **1985**, *107*, 3902−3909.

(32) (a) Wold, S.; Albano, C.; Dunn, W. J., III.; Edlund, U.; Esbensen, K.; Geladi, P.; Hellberg, S.; Johansson, E.; Lindberg, W.; Sjostrom, M. Multivariate data analysis in chemistry. *Chemometrics: Mathematics and Statistics in Chemistry*. Kowalski, B. R., Ed.; D. Reidel: Dordrecht, 1984; p 17. (b) Wold, S.; Ruhe, A.; Wold, H.; Dunn, W. J. The colinearity problem in linear regression. The partial least squares (PLS) approach to generalized inverses. *SIAM J. Sci. Statist. Comput.* **1984**, *5*, 735−743. (c) Clark, M.; Cramer, R. D., III. The probability of chance correlation using partial least squares (PLS). *Quantum Struct.-Act. Relat.* **1993**, *12*, 137−145. (d) Wakeling, I. N.; Morris, J. J. A test of significance for partial least squares regression. *J. Chemometrics* **1993**, *7*, 291−304. (e) Wold, S. In: van de Waterbeemd, H., Ed. *Chemometrics Methods in Molecular Design*; VCH: New York, 1995; p 195.

(33) ChemDraw Ultra 6.0, CambridgeSoft Corporation, 100 Cambridge Park, Cambridge, MA 02140.

(34) Bruncko, M.; McClellan, W. J.; Wendt, M. D.; Sauer, D. R.; Geyer, A.; Dalton, C. R.; Kaminski, M. A.; Weitzberg, M.; Gong, J.; Dellaria, J. F.; Mantei, R.; Zhao, X.; Nienaber, V. L.; Stewart, K.; Klinghofer, V.; Bouska, J.; Rockway, T. W.; Giranda, V. L. Naphthamidine urokinase plasminogen activator inhibitors with improved pharmacokinetic properties. *Bioorg. Med. Chem. Lett.* **2005**, *15*, 93−98.

JM050149R